AN ABSTRACT OF THE THESIS OF

David A. Tence for the degree of Master of Science in Mechanical Engineering presented on May 8, 1992.

Title: Dislodgement and Deformation of Microbubbles in Laminar Channel Flow

Redacted for Privacy

Abstract approved: _____

James R. Welty

In this thesis the critical parameters involved in the dislodgement and deformation of microbubbles in laminar channel flow, are determined and evaluated. Experimentally the effects of surface tension, viscosity, fluid flow rate, density, and bubble diameter on bubble dislodgement were evaluated. A theoretical scale analysis was performed which provided a general relationship between the parameters. Experimental results provided reasonable comparisons with values calculated from the scale analysis. Non-dimensional plots were generated of Weber number, at bubble dislodgement, versus Reynolds number and Weber number as a function of a non-dimensional bubble diameter. A calculated velocity detachment equation was also produced. This work is applicable to many areas of science and industry, particularly in the field of ink-jet printing.

Dislodgement and Deformation of Microbubbles in Laminar Channel Flow

by

David A. Tence

A THESIS

submitted to

Oregon State University

in partial fulfillment of
the requirement for the
degree of

Master of Science

Completed May 8, 1992

Commencement June 1992

APPROVED:

Redacted for Privacy

Professor of Mechanical Engineering in charge of major

Redacted for Privacy

Head of department of Mechanical Engineering

Redacted for Privacy

Dean of Graduate School

Date thesis is presented May 8, 1992

Typed by Researcher

ACKNOWLEDGEMENT

The author would like to thank professor J. R. Welty for the time and guidance spent in supervising and directing this project. I would also like to thank the Tektronix GPID ink-jet printer division for their funding of myself and the project. Special praise must be given to the people in the ink-jet printer division for their assistance while work was performed at Tektronix. In particular I would like to thank Dr. Ron Burr for the many hours spent consulting and guiding me on this project, and through who's insight enlightened me to the possibilities of fluid mechanics.

TABLE OF CONTENTS

LIST OF FIGURES

LIST OF FIGURES (continued)

LIST OF FIGURES (continued)

LIST OF TABLES

Dislodgement and Deformation of Microbubbles in Laminar Channel Flow

INTRODUCTION

The motivation behind evaluating the dislodgement and deformation of a small bubble comes from many branches of science and industry. The medical, pharmaceutical, and chemical industries are but a few that come to mind where the effect of a gaseous phase, in the form of bubbles, can be either hazardous or beneficial. In general wherever there is requirement for flow, steady or unsteady, of a single phase liquid, there is the potential for interference of this flow by a gaseous phase. The amount of interference by this gaseous phase depends on many factors such as flow requirements, liquid properties, and external environment. Identification and quantification of the critical parameters involved in bubble deformation and dislodgement, and development of theory explaining why this happens, will benefit any area of science and/or industry that is concerned with gaseous-liquid phase flow.

A particular example in industry, where interference of regulated flow by small bubbles can have a disastrous effect, is in the field of ink-jet printing. The concept behind ink-jet printing is that a single drop of liquid ink can be deposited on receptive medium, such as paper, at a

precise position in a particular moment of time. The process by which the ink is placed on the paper must be rapid, accurate, well coordinated and very reliable. It is conceivable that millions of these single drops are required to produce an image on a standard sheet of paper. If a small bubble is entrained in the flow portion of the ink-printer the deposition process may be significantly altered or destroyed. The basic mechanisms included in the flow portion of an ink-jet printer are a reservoir, flow passages, ink driving mechanism, and a small orifice. For reference a schematic representation of the flow portion is presented in figure 1. The reservoir contains the ink used for printing. Flow passages connect the reservoir to a driving mechanism which is usually placed in a small chamber. At the end of this small chamber are more flow passages connecting it to an external orifice.

To place a single droplet of ink on paper requires a series of coordinated events. First the orifice and paper must be mechanically adjusted to the correct position. Second the driving mechanism must produce a positive and negative regulated pressure pulse, for driving a small droplet of specific size out of the orifice, and pulling ink from the reservoir. Third the orifice and paper must be readjusted to the next position for printing. Because of the millions of single drops required to produce an image on a sheet of paper this process must happen within fractions

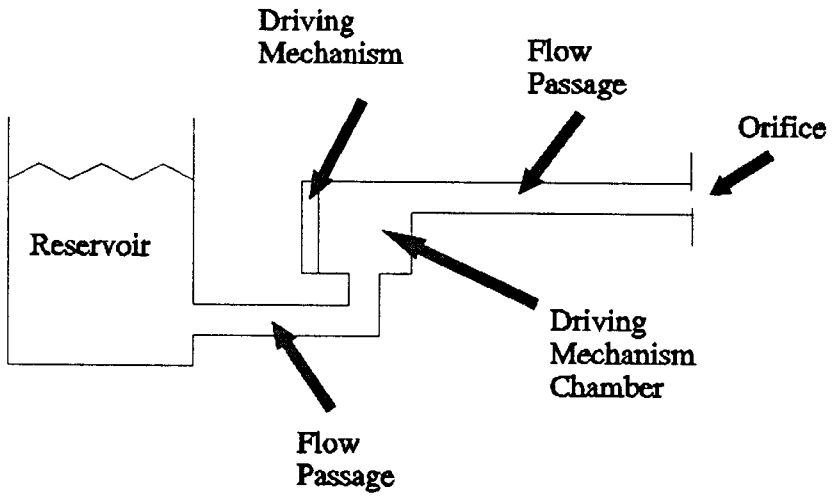

Figure 1. Ink-jet printer flow schematic

of a second. Thus reliability is of great concern.

If a small bubble is trapped in one of the flow passages, driving mechanism chamber, or next to the orifice it can disrupt the droplet output in a variety of ways. In any of these areas a trapped bubble can reduce or block the flow of ink thus preventing droplets from exiting the orifice. Also a bubble, located in the driving mechanism chamber or in a flow passage leading to the orifice, may totally or partially absorb the pressure pulse generated by the driving mechanism thus preventing or only partially allowing generation of droplets. In the later case, with the bubble partially absorbing the pressure pulse, it may

readmit the absorbed pressure pulse a fraction of a second later. This will result in two pressure pulses which can cause the generation of two droplets instead of one. A trapped bubble may also resonate if its size is such that the resonant frequency of the bubble matches that of the driving mechanism. In any of these cases the output of the droplet will be either blocked, reduced, or increased thus destroying the coordination and reliability of placing the droplet on the paper. The final result of this situation will be a distorted printed image, which is not the acceptable output of an ink-jet printer. Thus for ink-jet printing, which is a multimillion dollar per year industry, it is critical that all bubbles are dislodged and eliminated before printing takes place.

Typically this is done by a flushing process where large amounts of ink are forced through the flow system of the printer. In practice the amount of ink flushed through is determined by trial and error. If the critical parameters involved in the dislodgement and deformation of a microbubble could be determined, as well as an explanation developed, then the requirements for dislodgement would be known. This would enable a designer to specify the flow required to dislodge bubbles, or specify materials to use such that bubbles are easily dislodged. By knowing the critical parameters involved to dislodge a bubble, a designer could optimize the dislodgement process thus

increasing its effectiveness and reducing cost.

This thesis is concerned with identifying and quantifying the critical parameters, and their interrelationship, involved in the dislodgement and deformation of a small bubble in laminar channel flow. By doing so a means of predicting this behavior may be obtained.

Current Literature

In reviewing the current literature on dislocation and deformation of microbubbles no references were found that deal specifically with a single bubble in laminar channel flow. However, articles and texts were found which discuss physical relationships that influence dislodgement and deformation. Jansons developed an analytical model for moving contact lines on a two-dimensional rough surface, which seem to exhibit many of the observable characteristics of a moving contact line (Jansons, 1985). An experimental study was performed by Dussan on the ability of drops or bubbles to stick to a non-horizontal surface (Dussan, 1985). This study identified the critical value for the volume of the drop or bubble beyond which it will dislodge or move. Janczuk and Bialopiotrowicz examined the adhesion of an air bubble to a quartz surface in an aqueous solution of aliphatic amine hydrochloride (Janczuk, 1988). They measured the detachment force of an air bubble in relation

to the solution increase of the hydrochloride. De Gennes wrote a in-depth paper concerning wetting and other multiple phase phenomena (De Gennes, 1985). Ryskin and Leal performed numerical analysis on the buoyancy-driven motion of a gas bubble through a quiescent liquid (Ryskin, 1984). In their study they obtained complete solutions for Reynolds numbers in the range of 1 to 200 and Weber numbers up to 20.

In this thesis three general texts, which discuss different aspects of multiple phase phenomena, were used for explanatory references. These texts were Interfacial Phenomena (Miler, 1985), Liquid Vapor Phase Change Phenomena (Carey, 1992), and Wetting Spreading and Adhesion (Padday, 1978).

Project Approach

A four-step project approach was taken in this study to determine the critical parameters and theory, involved in dislodgement and deformation of microbubbles. The steps involved consisted of experimentation, theoretical analysis, computational simulation, and a literature search.

The experimental portion of the project entailed development of apparatus and test procedure for controlled dislodgement and deformation of microbubbles. The goal of this phase was to vary parameters such as flow rate, bubble size, surface tension, and fluid viscosity. The motivation for these chosen parameters is described in section on

Theoretical Scale Analysis. The requirements of the apparatus and test procedure were such that fluid flow, pressure, temperature, and bubble dislodgement were controlled or observed. Fluid properties such as surface tension, density, and viscosity were independently determined. For details of the apparatus and test procedure refer to the Apparatus and Procedures section.

In the experimentation, 219 test runs were made and recorded where bubble size, flow rate, viscosity, and surface tension were independently varied. In the Experimental Results section a discussion of the data and results are given. Also a presentation of the experimental results in the form of plots and processed data is made where the Weber number at bubble dislodgement is plotted versus the Reynolds number and non-dimensional bubble diameter. In this section experimental error is addressed as well as the general trends and conclusions that can be drawn from the obtained data.

The theoretical portion of this project is concerned with developing theory, describing the mechanisms behind dislodgement and deformation of small bubbles. One motivation behind developing theory is to provide a physical framework for evaluation of experimental results. Another is for prediction of dislodgement in fluids and flow regimes other than those evaluated in the experimentation. The approach taken was that of a rough scale analysis, which

resulted in the development of a more refined physical theory. From this analysis the critical parameters were determined. For verification of the analysis theoretical data was calculated and compared to the experimental results.

The computational portion of this project consisted of simulating a steady state flow model depicting flow past a "solid" bubble attached to a wall. By computationally simulating this flow field, insight was gained on pressure forces and fluid flow around and on the bubble. The computational simulation thus allowed for some verification of qualitative observations. The approach taken and the package used are discussed in the section on Computational Simulation.

A conclusion section is at the end of this thesis to discuss the different aspects of the project, new knowledge gained, application of the results, limitations of the study, and further research.

APPARATUS AND PROCEDURES

It was required of the experimental facilities that the critical parameters, involved in dislodgement and deformation of a microbubble, were able to be controlled and predictably changed. The identified parameters varied in the experiment were bubble size, fluid flow rate, fluid surface tension, and fluid viscosity.

The bubble diameters were varied from .8mm to 2.25mm. Fluid flow rates were increased from zero to the flow necessary for bubble dislodgement. Viscosity and surface tension were independently changed such that the experiment was performed on six different fluids of 1cp-72dyne/cm, 1cp-40.45dyne/cm, 1cp-31.65dyne/cm, 2.8cp-57.1dyne/cm, 3.8cp-45.4dyne/cm, and 19.6cp-48.54dyne/cm. For rationale behind varying these parameters, refer to the section on Theoretical Scale Analysis.

The experimental setup constructed consisted of a fluid flow test chamber, a pump, a flow meter, a reservoir, associated tubing to connect all parts, a thermometer, a microscope viewing system, a contact angle lens, video camera and recorder, a calibrated measuring system, and a bubble injection apparatus. This experimental setup allowed for the variation of bubble size and fluid flow rate. To modify surface tension and viscosity, surfactant and viscous liquids were added to the working fluid. For calibration of

the surface tension and viscosity a surface tension measuring instrument and viscometer were used.

Experimental Facilities

A schematic representation of the experimental setup is shown in figure 2. This schematic shows the general relationship of the parts which comprised the experimental setup. In figure 2 it is noted that for the highly viscous flow case the by-pass was not used, and a different pump was employed. A block portrayal of the actual setup for the highly viscous case is shown for reference in figure 3. The following is a detailed list of the individual components used for the setup and an estimation of their error where pertinent.

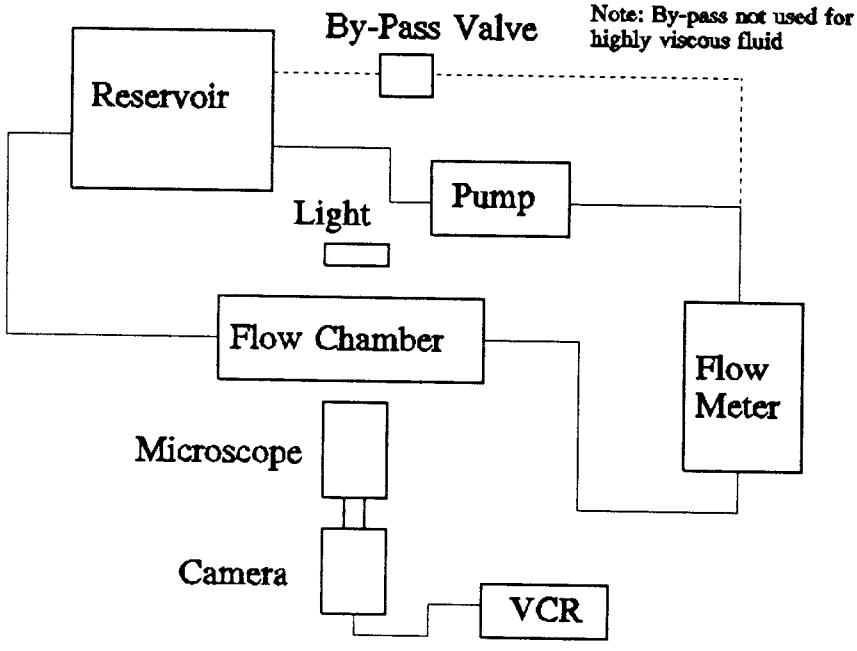

Figure 2. Schematic of experimental setup

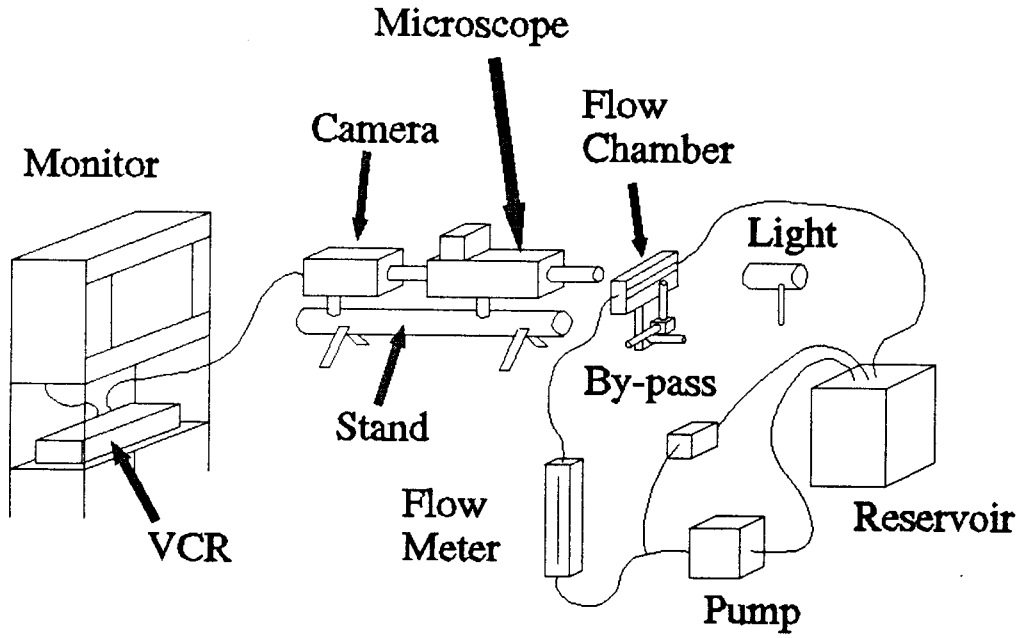

Figure 3. Block portrayal of actual setup

Flow Chamber-

The flow chamber is shown in figure 4. Essentially the flow chamber was constructed of two pieces of machined aluminum. The actual chamber as shown in the figure consists of a long narrow passage measuring 0.510-in wide, 0.145-in high, and 3.43-in long. The reason for the 3.5 to 1 ratio of width-to-height was to reduce side-wall effects on the bubble. At the ends of these passages are two settling chambers with an inlet and outlet at each end. The motivation behind designing the flow chamber with settling chambers was to reduce entrance effects, thus producing a steady fully developed laminar flow in the long narrow

passage. On the top and bottom of the long narrow passage was placed stainless steel strips, to allow for a consistent surface for bubble placement. The surface roughness on the strips were 3000 to 6000 angstroms, as measured by a Profilometer, alpha step 200. Each side of the flow chamber was constructed of plexiglass plates, so that the bubbles could be observed with the microscope video camera system. On the plate opposite the microscope a 1/4 inch hole was drilled, for injection of the of the bubble. Under the plexiglass plates are gaskets consisting of clear Tygon tubing. At the inlet and outlet, 1/8 inch brass hose nipple fittings were used for attachment of 1/8 inch Tygon tubing.

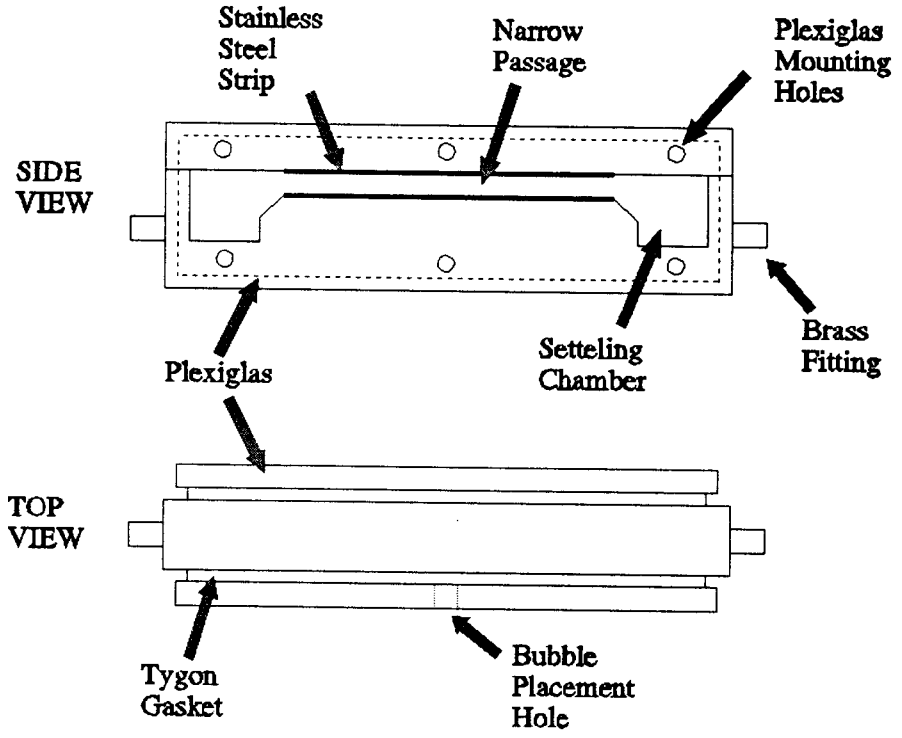

Figure 4. Flow chamber

Pump-

Two pumps were used in the experiment depending on the nature of the working fluid. For the standard and moderately viscous fluids the pump used was a SHURflo diaphragm pump model number 2088-403-444. This pump was rated at 2.8 GPM for 12VDC - 4 amps. Due to the high flow rate from the pump, the by-pass value was needed, as shown in figure 2. For the highly viscous fluid a 12VDC Roberk windshield washer pump, model P50 was used. Both pumps gave adequate performance with only minor fluctuation in the flow due to the pumping action. The power source used for both pumps was a LAMBDA power supply model LA-200, serial no. LA2-AA20-930.

Flow Meter-

A Dwyer 1-20GPH liquid flow meter, catalog no. RMB-83-SSU, was used to measure the flow rate of the liquid. This flow meter was of the rotameter type. To adjust the flow through the flow meter, and thus also the flow chamber, there was a flow meter control valve. Because the flow meter was calibrated for water in was necessary to calibrate for the liquids with different viscosities. This was done by setting the flow meter on a specific value and measuring the flow rate. Data used for the calibration is contained in the appendix. Estimated error for reading the flow meter was +/- 0.2 GPH.

Thermometer-

Temperature was measured with a type K thermocouple. The readings from the thermocouple were translated into temperature readings by a TEGAM microprocessor thermometer, model 821. The temperature averaged near 33 degrees celsius, varying only +/- 1.5 degrees. It was concluded, because of the small variation, that fluid properties were not affected by temperature variations. Temperatures values are listed in the appendix. Estimated error for the thermometer readings were +/- 0.1 degrees celsius.

Microscope Viewing System-

To view the microbubbles and record their dislodgement on video tape a Nikon SMZ-10 binocular microscope was used. The magnification was adjusted on the microscope such that a clear image was produced on the camera and associated video monitor. For illuminating the bubble a Tensor portable lamp, model C-2525, was used. In viewing the bubble it was necessary to adjust the contrast of the bubble with its surroundings. This was done by adjusting the position of the lamp.

Calibrated Measuring System-

To position the flow chamber and to determine the diameter of the bubble a three-axis micrometer system was used. The system is shown in block portrayal in figure 5. This system allowed for the bubble to be accurately positioned, and then moved a measured distance in any direction by reading the micrometers. The micrometer type

was Starrett, model numbers 263M and 63M. The resolutions for the micrometers were 0.01 mm. In general, once the bubble was initially positioned, only the x axis micrometer was used and read to determine the diameter of the bubble. Estimated error for bubble diameter measurement was +/- 0.01mm.

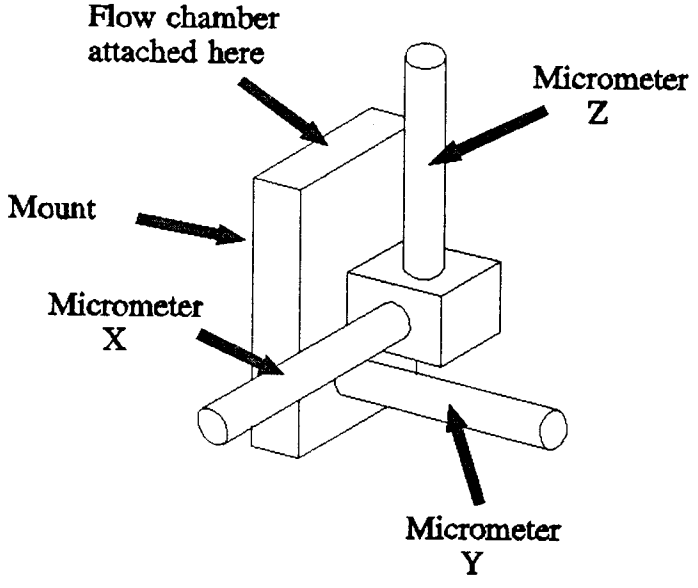

Figure 5. Three axis micrometer system

Contact Angle Lens-

To measure the bubble contact angle a lens from a Goniometer was used, model no. 100-00 115, Rame-hart, Inc. This lens has an internal adjustable protractor that is overlaid on the image seen from the microscope. By adjusting the protractor the bubble contact angle can be

measured. The contact angel was measured for use in the theoretical calculations, however, because of the large scatter in contact angle measurements, it was assumed the lens resolution was not sufficient for accurate measurements. For general observations on contact angle change, the video camera and recorder system were used.

Video Camera and Recorder-

Dislodgement and deformation of the microbubbles was recorded for all test runs using a black and white MTI-65 50/60Hz video camera attached to the microscope. The recorder used was a Mitsubishi VCR, model HS-U20, with an associated Sony 19 inch color television, model KV-1913. The contrast given by the black and white video camera was sufficient to determine, with certainty, bubble dislocation and dislodgement.

Bubble Injection Apparatus-

A syringe was used to place bubbles in the flow chamber. The syringe used was a Hamilton Gastight syringe, model number 1702, with a capacity of .025ml. The needle used was a Hamilton 26S Gage, model number 80427.

Viscometer-

Viscosity measurements were performed on a Brookfield Digital Viscometer, model LVTD serial number 1050. Estimated error for the fluid viscosity was +/- 0.1cp.

Surface Tension Measurement-

Surface Tension measurements were performed on a CAHN

Dynamic Contact Angle Analyzer, model DCA-312. Estimated error for surface tension was +/- 5 dyne/cm.

Fluids-

As mentioned, six different fluids were used in the experiment. Table 1 lists the different fluids, and the constituents used in making each batch. The tetraethylene glycol and the polyethylene glycol were both added to increase viscosity. The triton X-100 was added as a surfactant. Dowicil-75 is an antimicrobial.

Table 1. Fluid components

Fluid	Water	Comp. 1	Comp. 2
1cp-72dyne/cm	5285 ml		
1cp-40.45dyne/cm	5285 ml	Triton X-100 .15cc	
1cp-31.65dyne/cm	5285 ml	Triton X-100 .47cc	
2.8cp-57.1dyne/cm	3877 ml	Tetraethylene Glycol 1408 ml	
3.8cp-45.4dyne/cm	3523 ml	Tetraethylene Glycol 1762 ml	
19.6cp-48.55dyne/cm	2700 ml	Polyethylene Glycol 1273 g	Dowicil-75 .33 g

Test Procedure

In developing the test procedure, the goal was to develop a repeatable systematic method of gathering data.

The data gathered, as previously mentioned, were of fluid flow rate, bubble diameter, bubble dislodgement flow rate, fluid temperature, fluid viscosity, fluid density, and fluid surface tension. The test procedure consisted of two parts, that of bubble diameter versus flow rate, and the test for fluid properties.

Bubble Diameter versus Flow Rate-

For each fluid it was necessary to run a series of tests determining dislodgement flow rate for different bubble diameters. In these tests the deformation at different flow rates was recorded by the video camera recorder system. The bubble diameter was varied from 0.8mm to 2.5mm for each fluid, and a detailed numerical account of this variation is given as raw data in the appendix. The following lists the steps in a typical data acquisition test run for a single bubble diameter. It is noted that 219 test runs were performed for the experiment.

Step 1- The syringe plunger was displaced a specific amount such that it held a volume of air. This volume corresponded to an estimated bubble diameter, for example a 2 microliter displacement would correspond to an estimated bubble diameter of 1.5mm. By varying the displacement of the syringe, variation in bubble diameter was achieved.

Step 2- The needle of the syringe was inserted through the 1/4 inch hole in the side plexiglass plates (refer to figure AP-3), piercing the side gasket of the flow chamber.

Step 3- The syringe plunger was then depressed producing a bubble inside the flow chamber. In some cases it was necessary pull back on the plunger to produce a smaller bubble. The bubble was repositioned with the tip of the needle to the center of the flow passage. The rationale for positioning the bubble in the center, was to reduce side wall effects on the bubble, and allow for wall effects to be symmetric. In all cases the bubble was positioned on the top surface of the flow passage.

Step 4- The bubble was brought into focus on the video monitor of the video recorder system by adjusting its position. The rational behind adjusting the bubble position, rather than the microscope, was for the magnification of the bubble to remain constant. Lighting was adjusted to produce the best image on the video monitor of the video recorder system. The diameter of the bubble was then measured by adjusting the x-axis micrometer, and comparing the change to a reference mark on the video monitor. The contact angle of the bubble was measured by looking through the microscope, using the contact angle measuring lens.

Step 5- The VCR was turned on to record bubble deformation and dislocation. The fluid was then allowed to flow, increasing in increments of 1 GPH. The increases were marked on the video record by flashing the light a series of times corresponding to the flow rate. The flow rate was

increased until bubble dislocation occurred.

Step 6- Fluid temperature was recorded using the thermocouple measuring system. The temperature was measured every three test runs. The data for each test run in the form of bubble diameter, contact angle, bubble dislodgement flow rate, and fluid temperature were recorded.

Step 7- The system was reset for the next test run.

Fluid Properties Test-

After the test runs were completed for an individual fluid it was necessary to determine the fluid properties. As mentioned, the properties measured were density, viscosity, and surface tension. Density was determined by comparing the weight of the fluid to that of water, using a digital scale and a graduated cylinder. Viscosity was evaluated by testing a fluid sample in the viscometer, using the procedure outlined in the test manual for the Brookfield Digital Viscometer. Surface tension was measured by testing a sample in the CAHN Dynamic Contact Angle Analyzer, using the procedure outlined in its test manual. Both receding and advancing values for surface tension were measured. The average of these two values were used for the calculations.

Comments on Apparatus and Procedures

The apparatus developed and procedures used allowed for critical parameters, involved in bubble deformation and dislocation, to be controlled and predictably changed. Much

time and care were taken for the necessary 219 test runs. On average 25 minutes were needed to perform a single test run. After several test runs the flow chamber was disassembled and reassembled for cleaning, to assure consistent surface and prevent fluid contamination. With regard to errors in obtaining data, most came from resolution error and operator interpretation error. The exception to this was the surface tension measuring machine and the viscometer, which had associated equipment error.

EXPERIMENTAL RESULTS

The focus of the experimentation was to obtain data on the critical parameters affecting bubble deformation and dislodgement. The parameters chosen were fluid flow rate, bubble diameter, fluid density, fluid viscosity, and surface tension. The rational behind choosing these parameters can be attributed to the force balance on a bubble, where at bubble dislodgement the attaching forces equal the dislodgement forces. The force attaching a bubble to a wall results from the surface tension force, which is related to bubble diameter. A force acting to deform and dislodge the bubble can be attributed to the pressure force exerted by the fluid motion, which is related to fluid viscosity, bubble diameter, and density. Another dislodgement force is the viscous drag exerted on the bubble by the fluid, which is related to viscosity and bubble diameter. An in-depth description of this force balance and the resulting chosen parameters is given in the section on Theoretical Scale Analysis. From this analysis it follows that the chosen parameters of fluid flow, bubble diameter, density, viscosity, and surface tension are the appropriate ones to determine the necessary relationships to dislodge a bubble.

In the experiment 219 test runs were performed to obtain data. The process by which the data was obtained is explained in the section on Apparatus and Procedures. The

219 test runs were broken into six sections each consisting of a different fluid. Table 2 lists the different fluids and the number of test runs performed with each.

Table 2. Fluid number and test runs

Fluid	Surface Tension	Viscosity	Test Runs
1	72dyne/cm	1cp	58
2	40.45dyne/cm	1cp	38
3	31.65dyne/cm	1cp	37
4	45.4dyne/cm	3.8cp	30
5	57.1dyne/cm	2.8cp	29
6	48.5dyne/cm	19.6cp	27
		Total=	219

For the test runs, raw data collected consisted of bubble diameter in millimeters, flow rate in gallons per hour, density in grams per cubic centimeter, viscosity in centipoise, contact angle measurement, and surface tension in dynes per centimeter. Figure 6 and Figure 7 are plots of the data obtained in the form of the average channel dislodgement velocity versus the bubble diameter. The average channel dislodgement velocity is the flow rate divided by the cross sectional area of the channel. The figures show the required dislodgement velocity, in all the different fluid cases, tends to increase exponentially as the bubble diameter decreases.

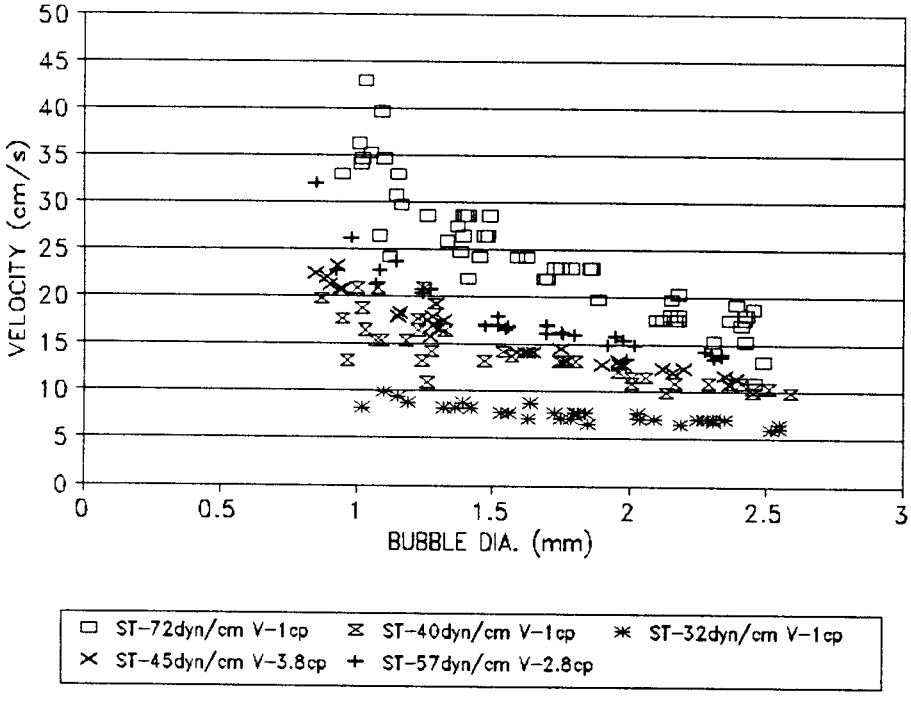

Figure 6. Channel velocity vs. bubble dia. fluids 1-5

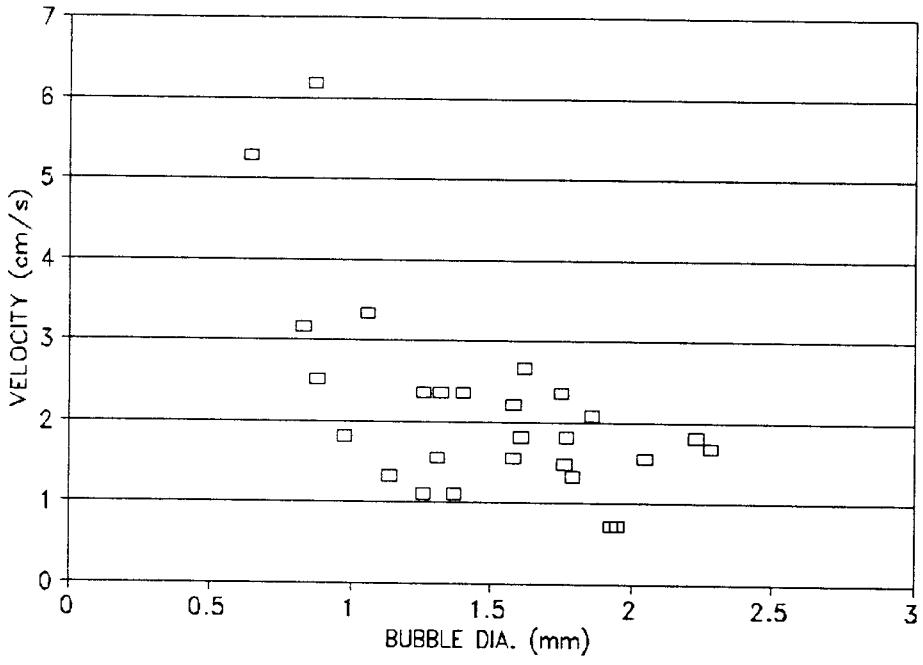

Figure 7. Channel velocity vs. bubble dia. fluid 6

Note the raw data is tabulated in the Appendix.

As mentioned in the Test and Procedures section it was necessary to calibrate the flow meter for the different viscosities. The equations used for the calibration and the raw data is contained in the Appendix.

The results from the experimentation are presented in two sections. The first deals with the general qualitative aspects observed for bubble dislodgement in all test cases. The second is a quantitative presentation, in non-dimensional parameter form, of the data obtained for the previously mentioned chosen dislodgement parameters. The

data was presented in this form so that the results may be applicable to cases and fluids, different than the ones tested. From the non-dimensional data presented, an estimate can be made as to the flow requirements for bubble dislodgement.

Qualitative Results

In all of the test runs made the same type of dislodgement phenomena were observed. Initially at zero flow, the bubble was placed on the top surface of the flow chamber. The contact angle, measured in the liquid, would be the same on both sides of the bubble. The shape of the bubble was spherical except for the portion in contact with the chamber top, which was flat. Refer to figure 8 part (a). As the flow was increased the contact angle on the side facing the increasing flow, the upstream side, would increase while the contact angle on the side away from the flow, the downstream side, would remain essentially the same. The shape of the bubble would deviate from spherical with the top slightly increasing in curvature, and the upstream face decreasing. Refer to figure 8 part (b). When the flow was increased to the point of bubble detachment the contact angle on the upstream side was observed to approach 90 degrees for the low and moderately viscous fluids (1cp, 2.8cp and 3.8cp), and 80 degrees for the highly viscous fluid (19.6cp). The contact angle on the downstream side

still was observed to remain essentially the same. The shape of the bubble had changed even more, with top curvature still increasing and upstream face curvature decreasing. Refer to figure 8 part (c). When the flow was increased after the maximum contact angle had been reached the bubble would fully detach from the wall, again becoming spherical and move with the fluid, or the bubble would move along the wall, maintaining the maximum contact angle on the upstream side of the bubble.

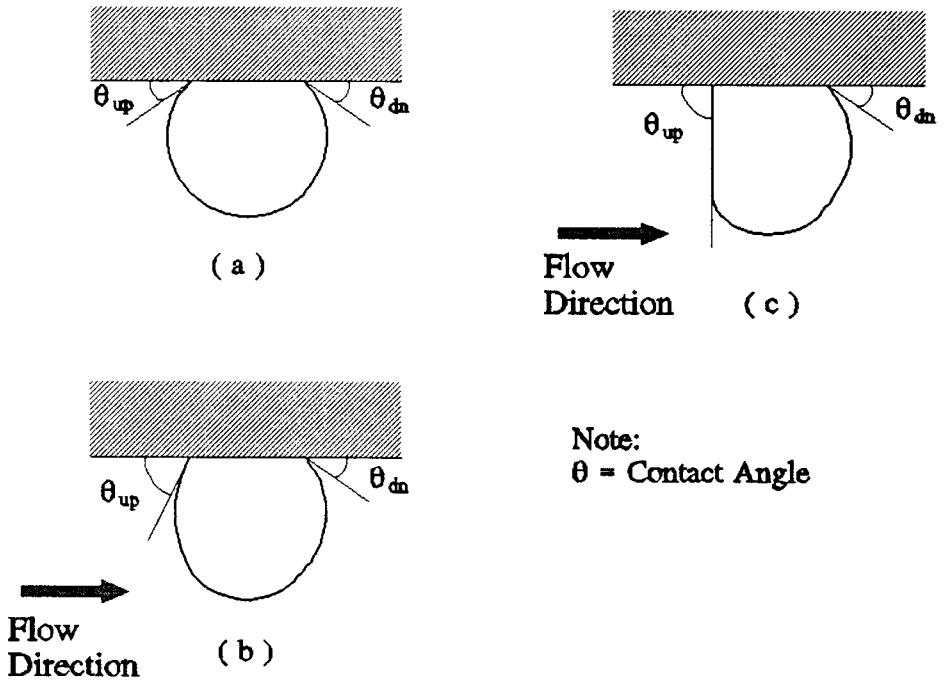

Figure 8. Bubble dislodgement

In general it was observed that after the flow was initiated, a recirculation zone developed on the downstream side of the bubble. This recirculation zone would become

larger and stronger as the flow increased. Also it was noticed that the surface of the bubble was circulating, again getting stronger as the flow increased. Note these observations were made by viewing very small microbubbles caught in the recirculation zones.

The bubble was only observed two dimensionally due to the nature of video monitor used to record bubble detachment. In reality the situation is three dimensional thus the contact angle and shape of the bubble must change smoothly from one side to the other. Note the contact line is the line the bubble makes with the top surface, at the point of bubble wall attachment.

An explanation behind the described change in contact angle and dislocation of the bubble is given in the section on Theoretical Scale Analysis. In regards to the slight bubble deformations, Liquid Vapor Phase Change Phenomena gives an explanation in the form of the Young-Laplace equation (Carey, 1992).

Young-Laplace equation:

$$\Delta P = \sigma \left[\frac{1}{r_1} + \frac{1}{r_2} \right]$$

Where:

ΔP = is the pressure difference across the bubbles surface

r_1 = radius of curvature along the first spherical angular coordinate

r_2 = radius of curvature along the second spherical angular coordinate

σ = the surface tension

Essentially what the Young-Laplace equation states is that an increase in pressure on the surface of a bubble will result in a decrease in curvature, while a decrease in pressure will result in an increase in curvature. What is observed in the experimentation is a decrease in curvature on the front face and an increase on the top. Thus the implication is, when flow is increased, pressure increases on the upstream face and decreases on the top.

Quantitative Results

It was decided to present the data in non-dimensional form. The rational was to enable the results to be applicable for fluids other than the ones tested upon. The non-dimensional parameters chosen to plot were the Weber Number versus the Reynolds Number and the Weber Number verses a non-dimensional bubble diameter. The Weber Number was chosen since it is a ratio of the pressure forces on the bubble to the surface tension forces, these are two main forces involved in the dislodgement force balance. The Reynolds number was chosen since gives an indication of the extent of the viscous force on the bubble, the other force involved in the force balance. For reference the following lists the Weber Number and Reynolds number.

Weber Number (We) and Reynolds Number (Re):

$$We = \frac{\rho d V^2}{\sigma} \qquad and \qquad Re = \frac{\rho d V}{\mu}$$

Where:

ρ = density

d = bubble diameter

V = local fluid velocity

σ = surface tension

μ = viscosity

In the data presented, the non-dimensional bubble diameter is a ratio of the measured bubble diameter to the channel height. Thus:

$$Bubble\ Dia.\ (non\text{-}dim) = \frac{Bubble\ Dia.\ (actual)}{Channel\ Height}$$

The velocity used in the Reynolds and Weber number were the estimated average velocity seen by the bubble. This velocity was calculated from the average channel velocity using the assumption that for laminar channel flow a parabolic profile exists. From White's Viscous Flow the maximum channel velocity can be found, from the ratio of the maximum channel velocity to the average channel velocity (White, 1991). The following equation was used for average flow velocity on the bubble.

$$V_{AVE} = V_{MAX}\left[\frac{2d}{W} - \frac{4d^2}{3W^2}\right]$$

Where:

d = the bubble diameter

W = channel width

$V_{AVE} = .552 * V_{MAX}$

This equation can be derived by integrating the velocity profile seen by the bubble, and dividing by the bubble diameter.

Figures 9-14 plot the local Weber number versus the local Reynolds number. Figure 15 is a composite of figures 9-13, to show a comparison of the data for the low and moderately viscous fluids. Figure 16 is another composite plot of the data for moderately viscous fluids, except the viscosity in the Reynolds number has been scaled by the following velocity scale ratio.

$$Re = \frac{\rho DV}{\mu_{fluid}} X \frac{\mu_{fluid}}{\mu_{water}}$$

Note the apparent linear relationship in figure 16 follows the relationship (We= 0.003618*RE - 0.04251).

Figures 17-22 are plots of the Weber number versus the non-dimensional bubble diameter. Figure 23 is a composite plot of figures 17-21 to show a comparison of the data for low and moderately viscous fluids. The fluid numbers in figures are those stated in Table 2.

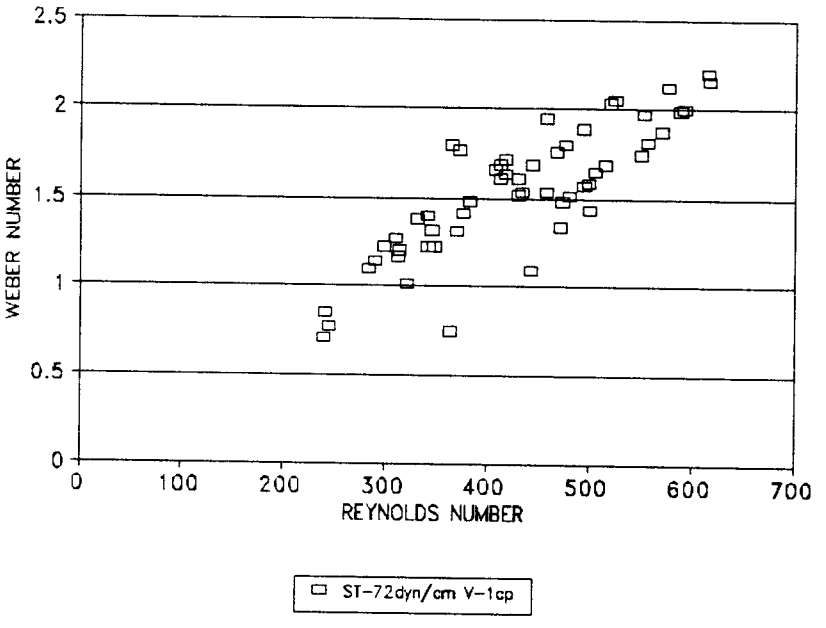

Figure 9. Weber vs. Reynolds number - fluid 1

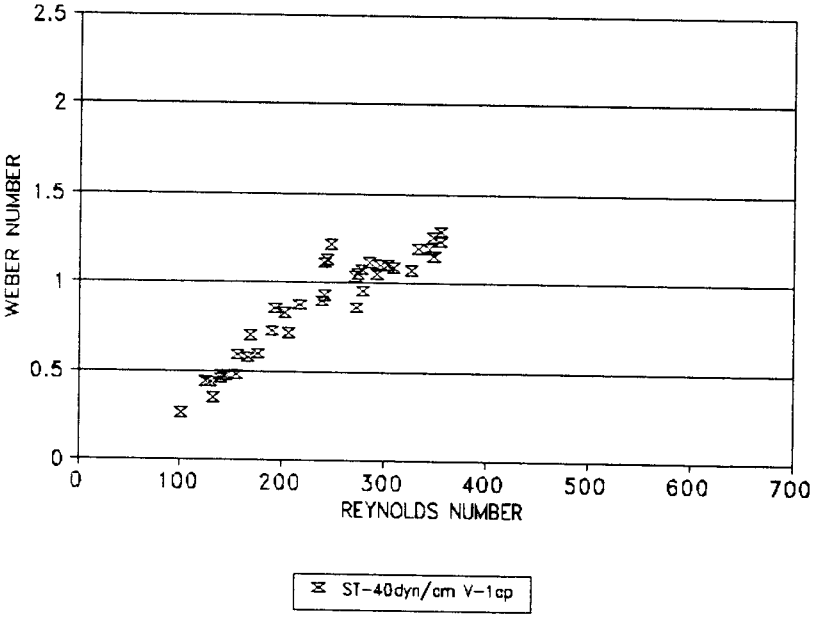

Figure 10. Weber vs. Reynolds number - fluid 2

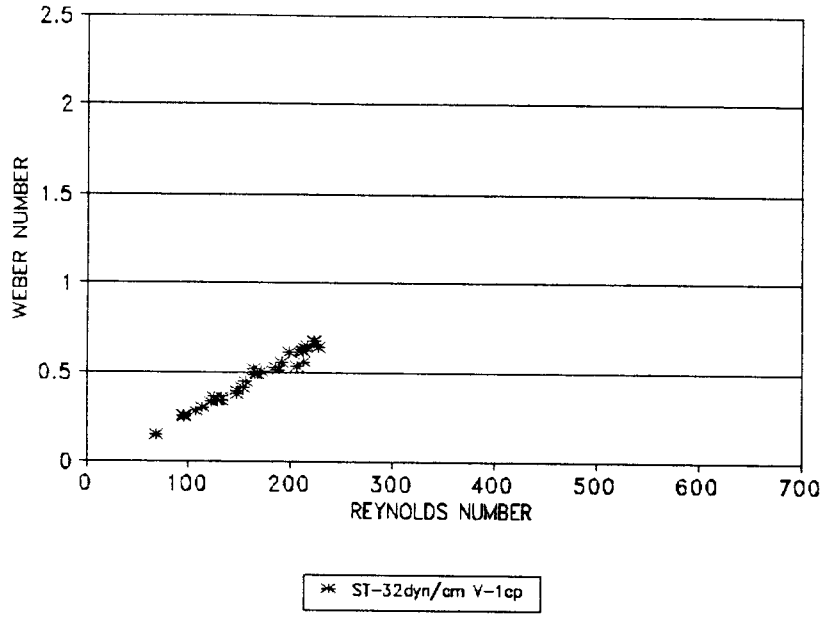

Figure 11. Weber vs. Reynolds number - fluid 3

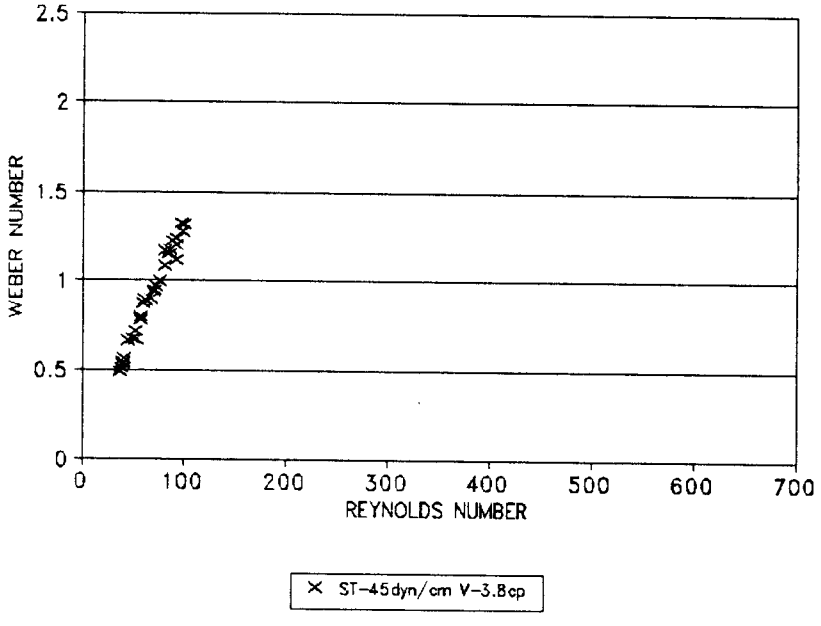

Figure 12. Weber vs. Reynolds number - fluid 4

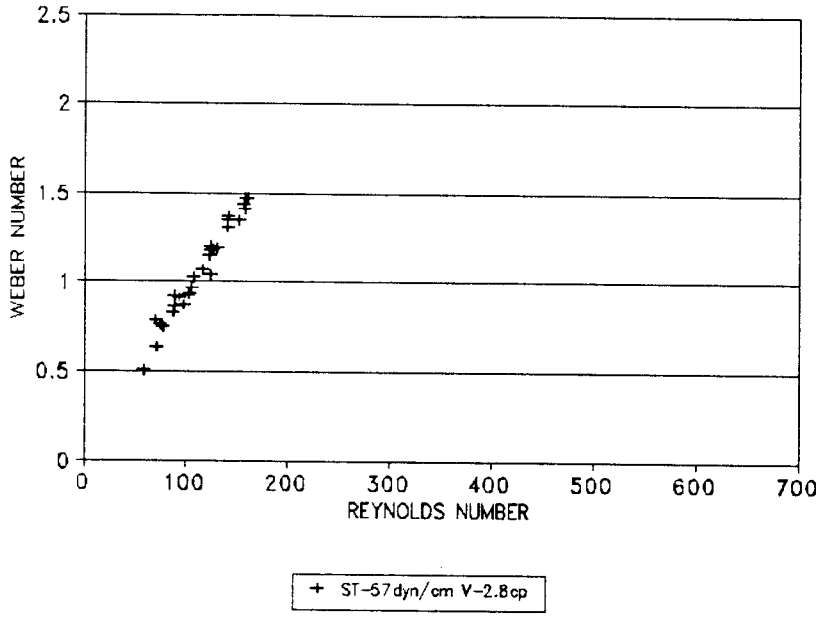

Figure 13. Weber vs. Reynolds number - fluid 5

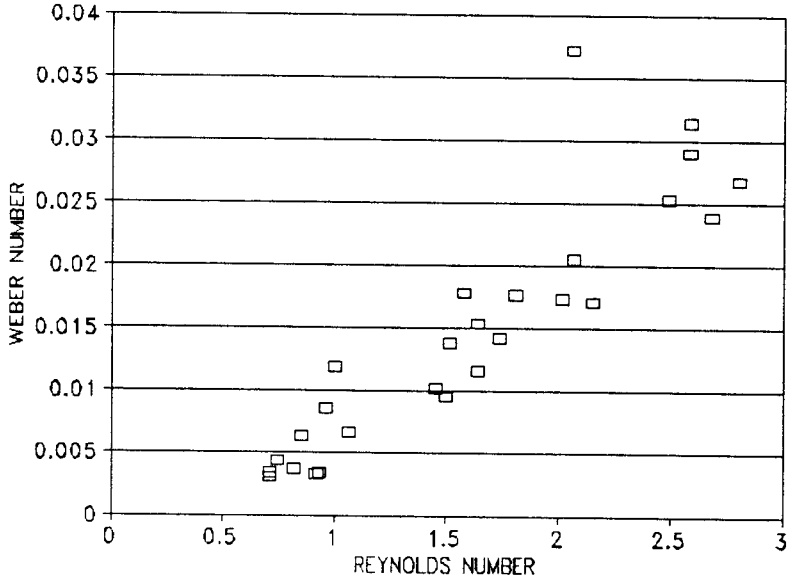

Figure 14. Weber vs. Reynolds number - fluid 6

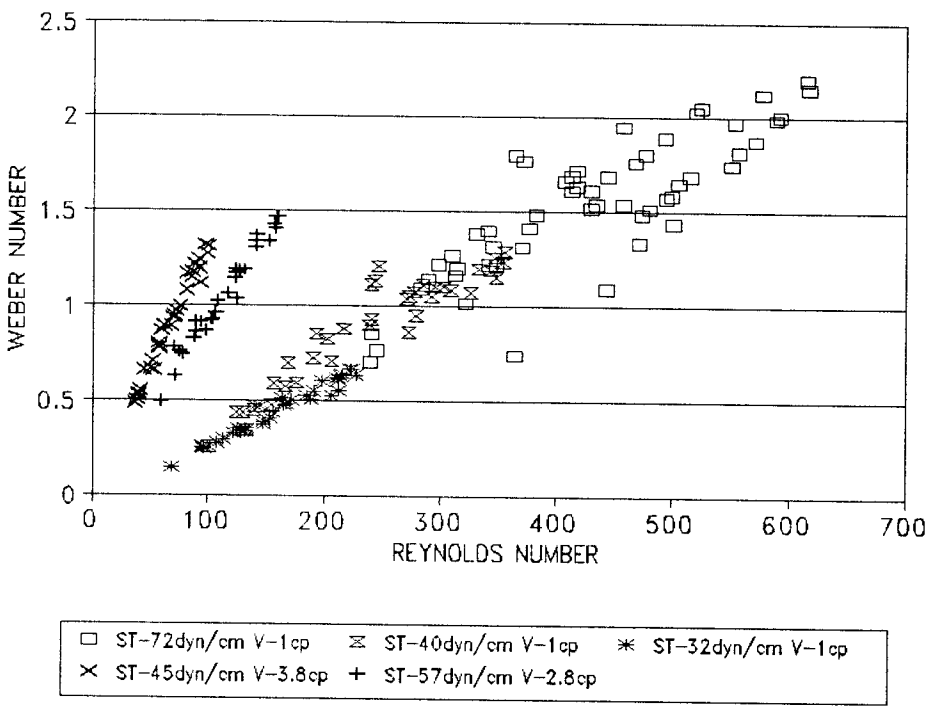

Figure 15. Composite of We vs. Re - fluids 1-5

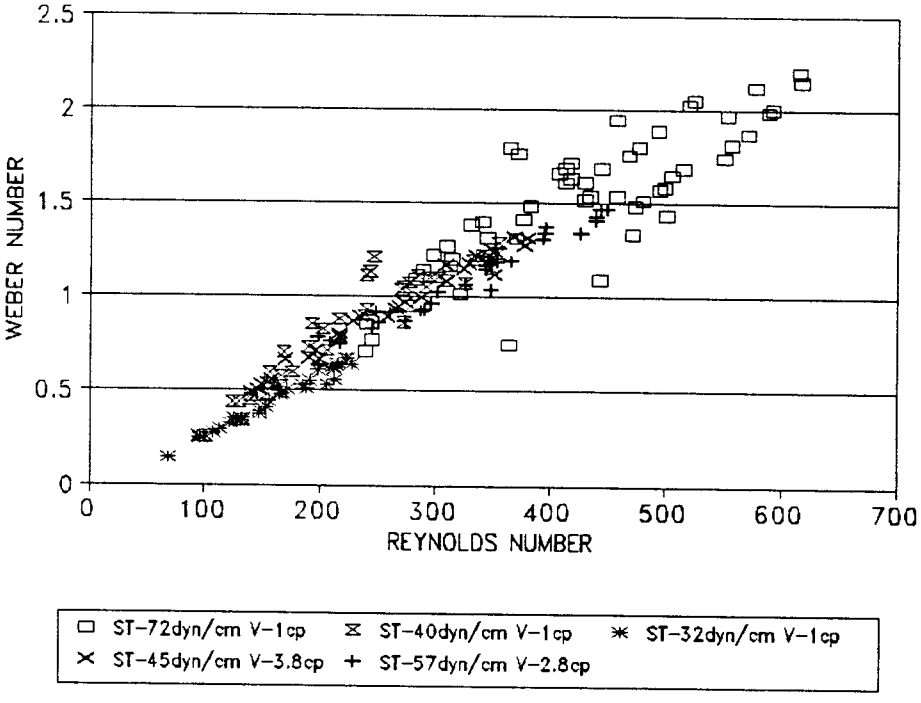

Figure 16. Comp. of We vs. Re scaled visc. - fluids 1-5

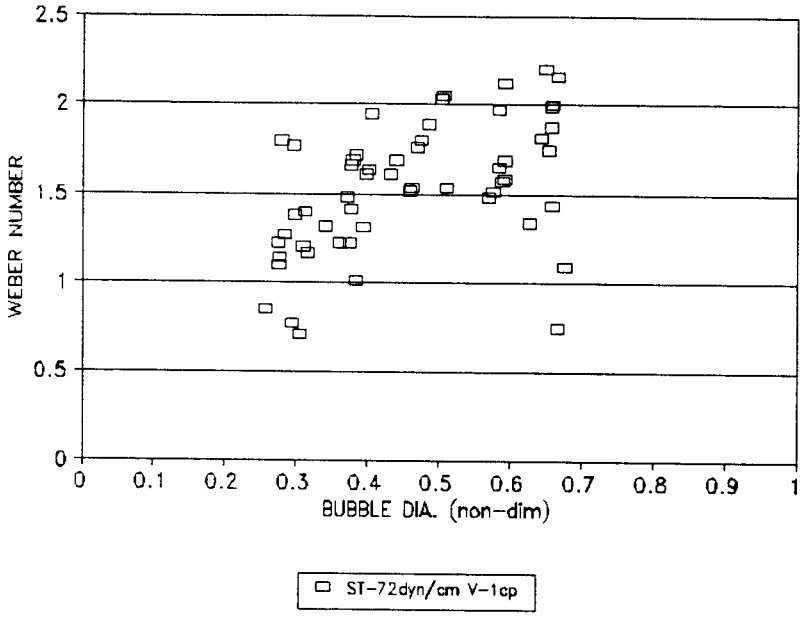

Figure 17. We vs. non-dim. bubble dia. - fluid 1

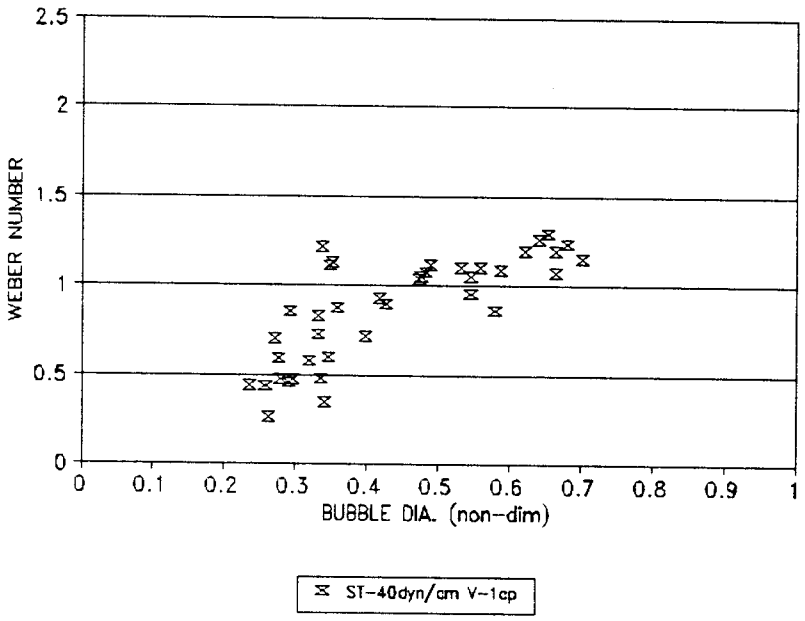

Figure 18. We vs. non-dim. bubble dia. - fluid 2

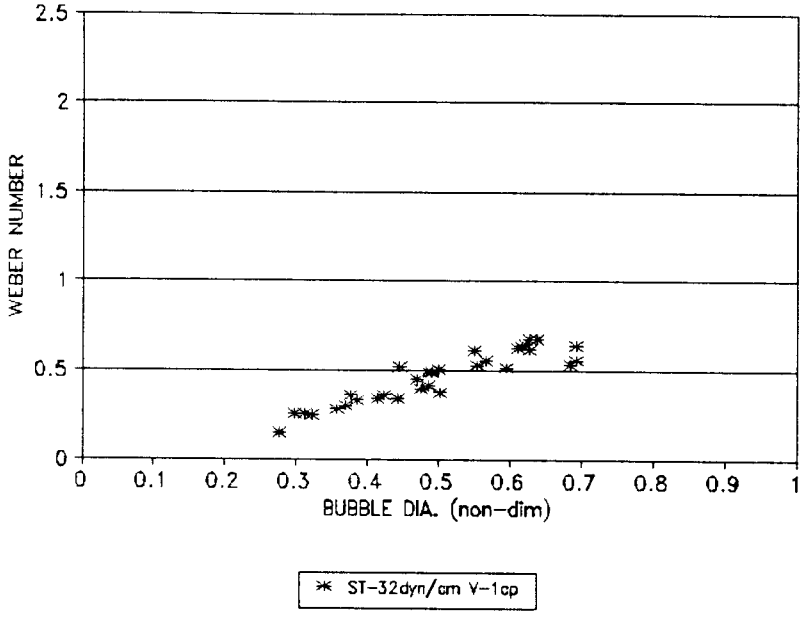

Figure 19. We vs. non-dim. bubble dia. - fluid 3

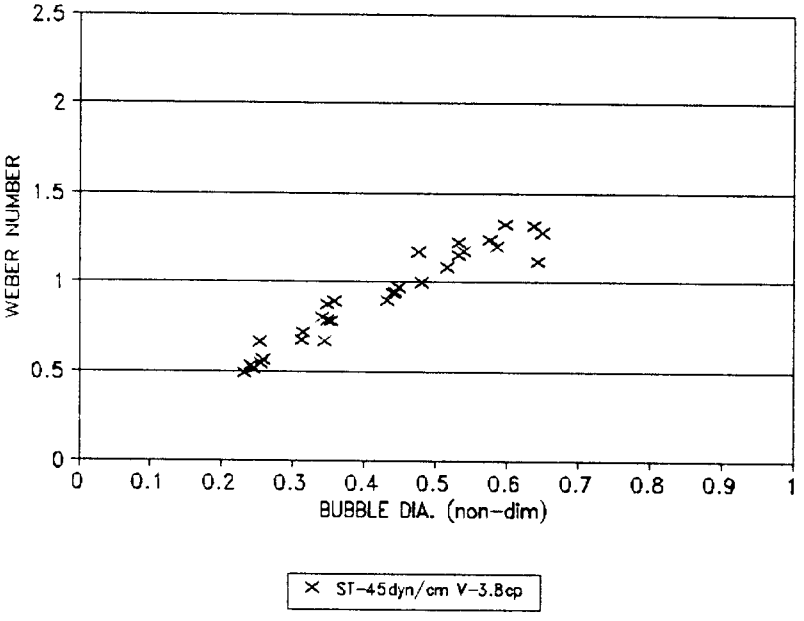

Figure 20. We vs. non-dim. bubble dia. - fluid 4

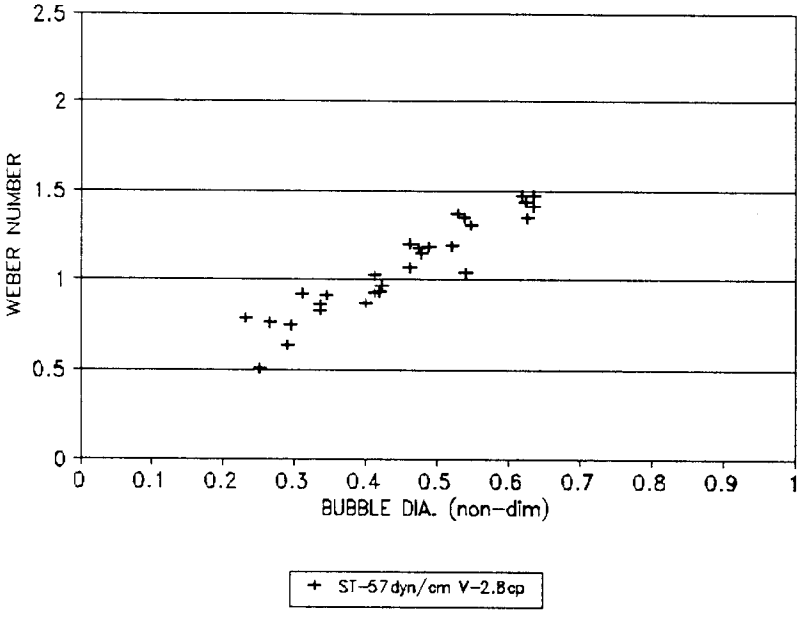

Figure 21. We vs. non-dim. bubble dia. - fluid 5

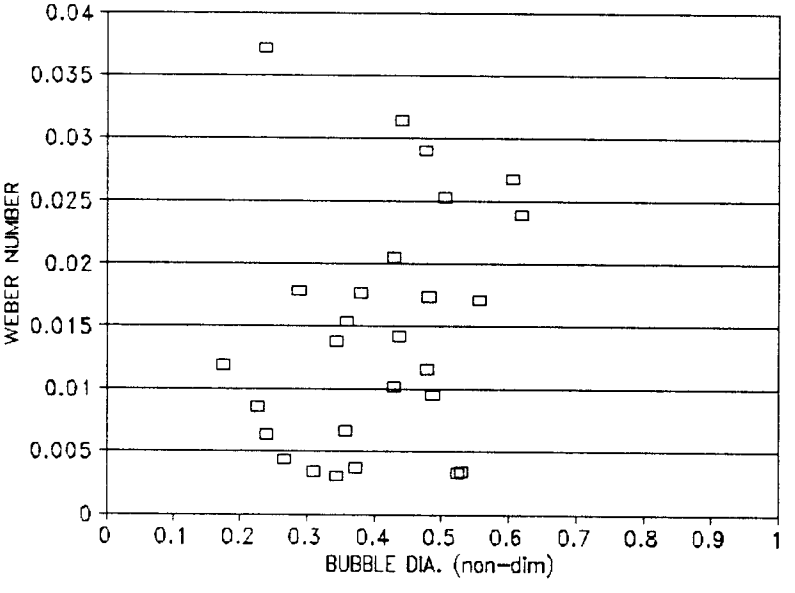

Figure 22. We vs. non-dim. bubble dia. - fluid 6

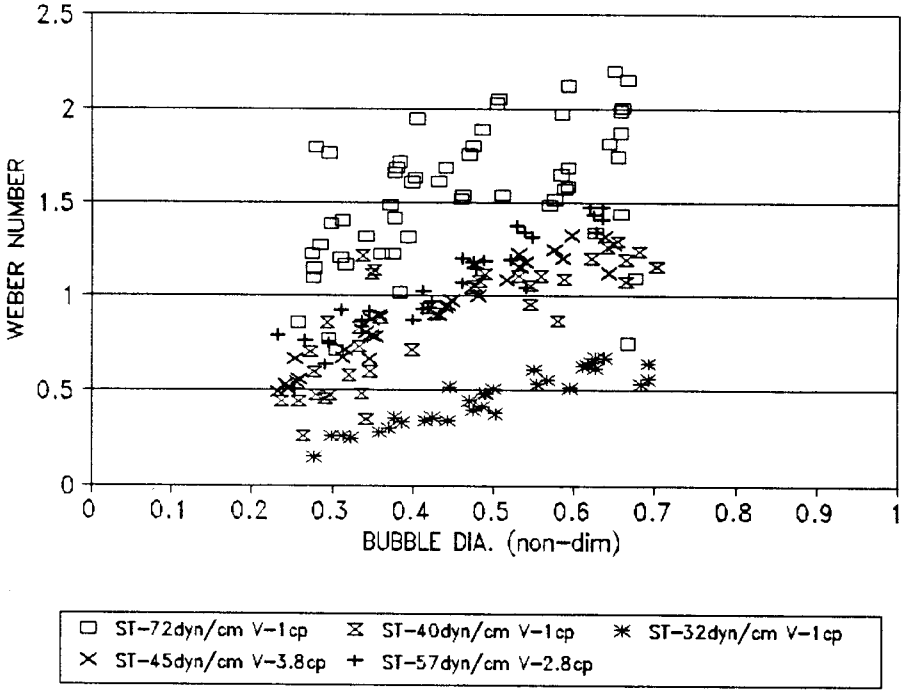

Figure 23. Composite of We vs. non-dim. bubble dia. - fluids 1-5

Error Estimation

In obtaining the raw data for the experiments, measurement errors were encountered for the chosen critical parameters of flow rate, bubble diameter, fluid density, chamber height, surface tension, and fluid viscosity. Table 3 lists the critical data and the estimated measurement error associated with it. The formulas used to calculate error were as follows, where % represents the percentage error in the particular value.

$$\%We = \%\rho + \%d + (2 * \%V) + \%\sigma$$

$$\%Re = \%\rho + \%d + \%V + \%\mu$$

$$\%\text{Non-dim. bubble dia.} = \%d + \%\text{channel height}$$

These formulas pertain to the error calculation for all of the measured parameters. A more accurate representation, for the error would be to use the percentage error from the bubble diameter and flow rate. The rational for better accuracy is, for each test run the flow rate and bubble diameter were measured, unlike the other parameters. Table 3 gives the average calculated percentage error in the Weber number, Reynolds number, and the non-dimensional bubble diameter for both cases of the error calculation.

Comments on Experimental Results

By analyzing the critical parameters, involved in bubble dislodgement, it was possible to predict when behavior occurs. Figures 9-23 seem to give a good

Table 3. Estimated error

Measured or Calculated Parameter	Error (+/-)
Flow Rate	.2 gph
Bubble Diameter	.05 mm
Fluid Density	.03 g/cm^3
Cross Sectional Area	1.06 mm^2
Channel Height	.127 mm
Surface Tension	3 dyne/cm
Fluid Viscosity	.1 cp
Weber Number (full calculation)	16.9 %
Weber Number (accurate calculation)	9.6 %
Reynolds Number (full calculation)	16.5 %
Reynolds Number (accurate calculation)	6.5 %
Non-Dimensional Bubble Diameter	6.8 %

experimental results for the prediction of bubble dislodgement. In figures 9-14 the local Weber number versus Reynolds number is presented. Generally the data for each of the plots seems to predict a linear relationship between the Weber and Reynolds number. In the composite plot, figure 15, this linear relationship is more apparent. It is noticed that data for the fluids with the same viscosities are on the same linear curve. Figure 16 is another composite plot of figures 9-13, except the Reynolds number has been multiplied by the viscosity scale ratio, so that the scaled Reynolds number does not reflect differences in viscosity. The linear relationship of the Weber number to

Reynolds number is even more apparent in figure 16 with all the data lying on the same linear curve.

By scaling out the viscosity for the low and moderately viscous fluids, and then having the results show excellent data correlation, indicates the viscous drag force has little effect on bubble dislodgement. This should be expected since the Reynolds number for these fluids are in a range from 50 to 600, which generally indicates viscous drag is small in comparison to form drag, refer to Viscous Flow page 184 (White, 1991).

Figure 16 can be used as a tool to estimate, for low and moderately viscous fluids, bubble dislodgement or attachment. Data points plotted above the curve indicate bubble dislodgement while data points plotted below indicate attachment. Thus for prediction of a bubble dislodgement flow regime, all that one needs to know is the fluid surface tension, density, and viscosity and then pick an appropriate smallest bubble diameter and local fluid velocity such that the Weber versus Reynolds number relationship places the data point above the curve.

Figures 17-22 plot the Weber number versus the non-dimensional bubble diameter. By plotting the data this way the dependance on viscosity is eliminated. In figures 17-21 there seems to be a somewhat linear dependance of Weber number on the non-dimensional bubble diameter. However, it is noticed that the groupings of data for the different

fluids are independent. These grouping follow the trend that as the surface tension is increased, an average higher Weber number is seen. Figure 23 is a composite of figures 17-21.

In figure 22, which is a plot for the high viscosity fluid, the linear dependance between the Weber number and non-dimensional bubble diameter does not exist. In fact the data seems to be scattered. Figure 14, a plot of Weber versus Reynolds number for the high viscosity data, shows the same data having a linear relationship to Reynolds number. Thus unlike the low and moderately viscous fluids, bubble dislodgement for the high viscosity fluids seams to be dependant on viscosity. Again this should be expected, since low Reynolds numbers, in the range of 0.5 to 2.5, indicate viscous drag forces are very important in comparison to form drag, this again is discussed in Viscous Flow (White, 1991).

Figures 17-21 and 23 can be used to predict bubble dislodgement. However, they are not as useful as figures 9-16, since a different Weber number grouping results for the fluids with different surface tensions.

THEORETICAL SCALE ANALYSIS

The goal of the thesis was to determine the critical parameters involved in the dislodgement and deformation of a microbubble, attached to a surface in laminar channel flow. A starting place for determination of these parameters would be to estimate the forces involved. By performing a force balance between the attaching and detaching forces one should be able to not only determine the critical parameters, but also develop a basic scale analysis theory to predict bubble dislodgement.

In the theoretical analysis three main forces, involved in bubble dislodgement, will be evaluated. The first is an attachment force, which is due to the surface tension between the liquid vapor interface. This surface tension, acting along a contact line the bubble makes with the surface, creates a force that resists bubble detachment. The second force, a detachment force, is due to pressure from the flow of fluid on the bubble. This force is essentially form drag on the bubble. The third force, another detachment force, is viscous drag due to flow of a viscous fluid on a bubble. For visual depiction of these forces refer to figure 24. A force balance can be written that will consist of the following:

Surface Tension Force = Form Drag + Viscous Drag

Two other forces involved in bubble dislodgement are

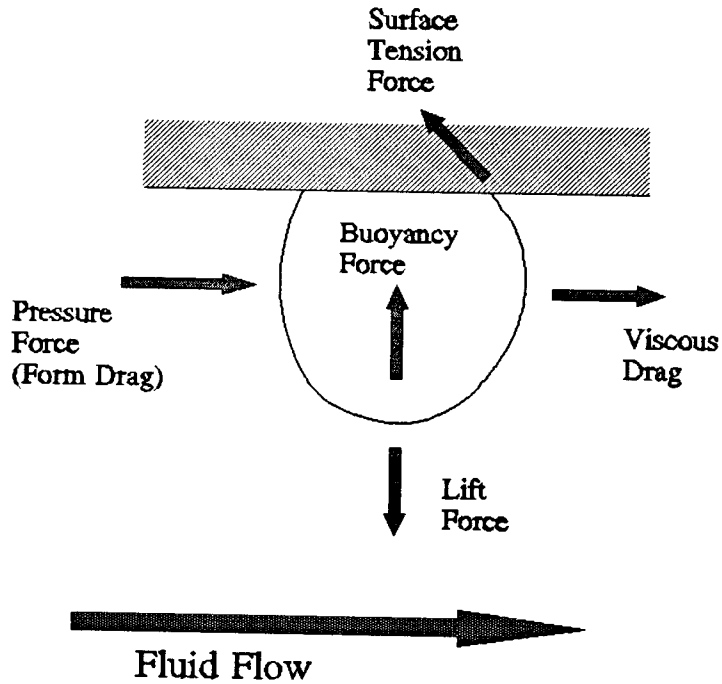

Figure 24. Attaching and dislodgement forces on bubble

the buoyancy force and the lift force on the bubble. Because the experiment was performed on a top horizontal surface, both of these forces would be in a vertical direction, with the buoyancy force opposing the lift force. Because both forces are vertical in the experiment, they would not resist a horizontal detachment force, refer to figure 24. Thus for the sake of comparing the theoretical results to the experimental, these forces have been ignored. If however one is to determine the flow requirements for bubble dislodgement in cases of a non-horizontal or bottom horizontal surface, buoyancy and lift forces should be included.

To calculate the form drag and viscous force on the

bubble the concept of a drag coefficient can be employed. From Welty, Wicks, and Wilson an equation is given for the force on a body due to fluid flow (Welty, 1984). Thus the drag force is:

$$F = A_p C_D \frac{\rho V^2}{2}$$

Where:

C_D = the drag coefficient

A_P = the projected area ($\pi d^2/4$)

V = the local velocity

The drag coefficient incorporates the effects of both form drag and viscosity, such that for high Reynolds number only form drag is present while for low Reynolds number viscous drag is the dominating effect. The drag coefficient is essentially a function of Reynolds number and thus is strongly determined by viscosity. It can be written in the following form:

$$C_D = f(Re) = f(\frac{\rho dV}{\mu})$$

To calculate the attachment force due to surface tension one must examine its effect on the bubble. When viewing the interfacial contact line between the bubble and the solid there are three surface tensions involved, see figure 25. The three surface tensions are that of solid-liquid, liquid-vapor, and solid-vapor. If it is assumed that the interfacial tensions can be taken as forces, a

force balance can be written in the horizontal direction for the contact line. This force balance results in Youngs equation, for reference see Interfacial Phenomena (Miller, 1985). Thus for Youngs equation:

$$\sigma_{SV} = \sigma_{SL} + \sigma_{LV}\cos\theta$$

Where:

σ = the surface tension

θ = the contact angle

Note contact angle is measured in the liquid, see figure 25.

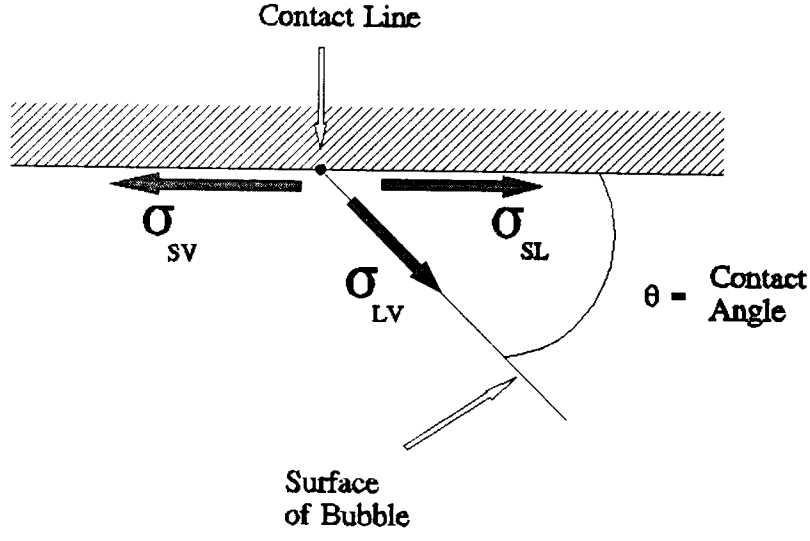

Figure 25. Contact line surface tension forces

In the experimentation it was observed that as flow was increased, the contact angle on the upstream side of the bubble would approach 90 degrees, while the downstream side

contact angle would remain relatively unchanged, see figure 8. This gives rise to a concept that by increasing the angle on the upstream side of the bubble, a net horizontal force is developed to resist drag due to fluid flow. Figure 26 pictorially shows this concept.

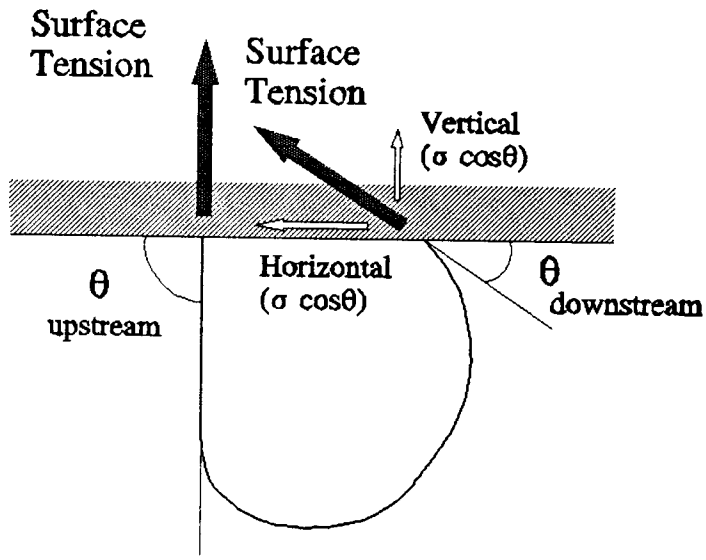

Figure 26. Bubble attachment forces

In the figure, the liquid-vapor surface tension force acts on the downstream side of the bubble to produce a horizontal and vertical component. On the upstream side, because the contact angle is 90 degrees, only a vertical component exists. Thus a net horizontal force is developed due to surface tension. It is noted that figure 26 shows the bubble two dimensionally, the actual force acts along a

contact line of which the contact angle must transition smoothly from the downstream to upstream side.

An estimation can be made for the net horizontal force by assuming both it acts only on the downstream half of the contact line, and the contact angle remains relatively unchanged for the downstream half of the bubble. Thus the horizontal component of the surface tension force can be calculated by multiplying surface tension and the cosine of the contact angle, refer to figure 26.

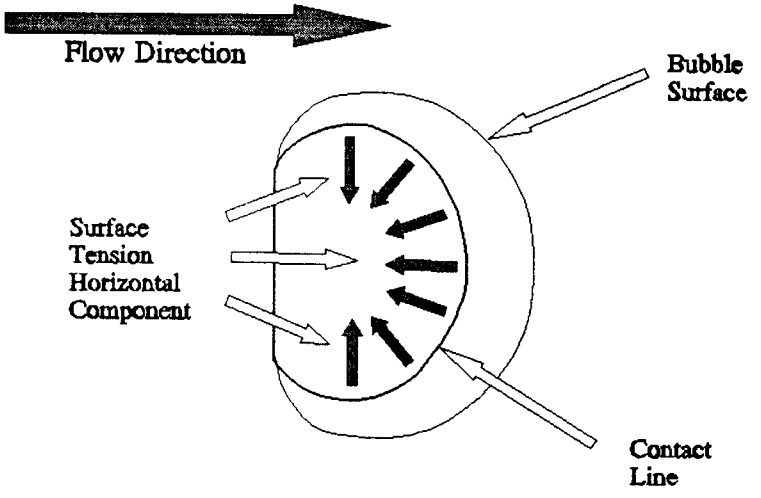

Figure 27. Bubble top view - horizontal surface tension components

Figure 27 shows that the horizontal component acts perpendicular to the contact line and thus only a component of the force, in the direction of the upstream half, is able

to resist drag. The other component cancels with a component from the other side of the bubble, see figure 28. To find the net horizontal force all the components in the upstream direction must be added along the down stream half of the contact line.

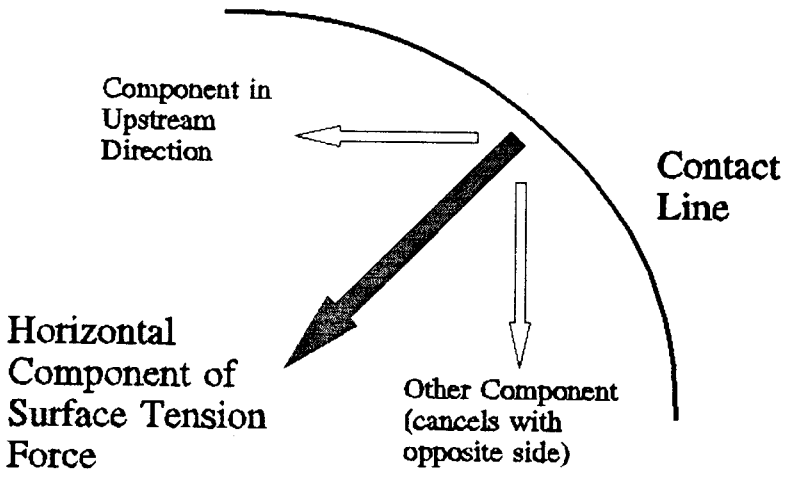

Figure 28. Components of horizontal surface tension component

The equation, shown below, resulting from the component addition can be used to find the net horizontal force.

$$Force = 2\int_0^{\pi/2} componet\ ds = 2\int_0^{\pi/2} \sigma\cos\theta\ \cos\phi\ r d\phi$$

Where ϕ is the angular measurement from the downstream direction to the upstream direction. The contact line radius r, which can be found by multiplying one half the

bubble diameter by the sine of the contact angle, is shown in figure 29.

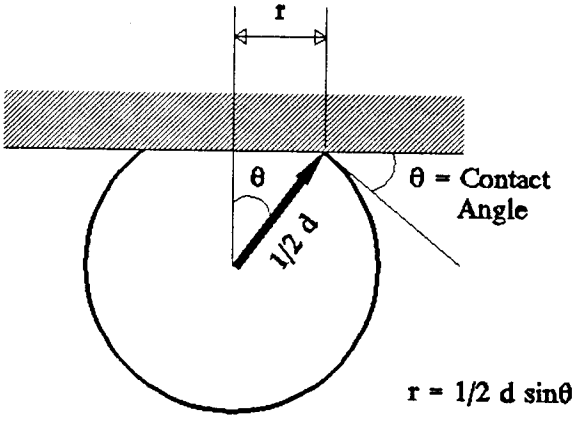

Figure 29. Contact line radius

Thus after substituting for r and integrating the equation for the net horizontal attachment force becomes.

$$Force = \sigma d \cos\theta \sin\theta = \sigma \frac{d}{2} \sin 2\theta$$

Theoretical expressions have now been obtained, which in a scale analysis sense, should approximate the attachment and detachment forces. The force balance involved for bubble detachment can be expressed in equation form using these two expressions. Thus:

$$\frac{\pi d^2}{4} C_D \frac{\rho V^2}{2} = \sigma \frac{d}{2} \sin 2\theta$$

This expression can in turn be solved for local velocity required to detach a bubble. Thus:

$$V = \sqrt{\frac{4\sigma \sin 2\theta}{\pi d C_D \rho}}$$

In deriving the above equation an assumption was made, based on observation, that the contact angle changes on the upstream side of the bubble as the fluid flow increases. This essentially is what allows for the net horizontal surface tension force to resist the drag force. The observation of the contact angle increasing, however, does not agree on macroscopic level with Youngs equation. The reason for this is Youngs equation gives a force balance of the surface tension forces in relation to the contact angle. Since the surface tension forces should not greatly change in a system, a change in the contact angle would result in a non-equilibrium situation. This apparent non-agreement of theory with observation can be explained by the theory of contact angle hysteresis, as explained in Interfacial Phenomena (Miller, 1985) and Liquid Vapor Phase Change Phenomena (Carey, 1992).

Figure 30 pictorially demonstrates how Youngs equation can be satisfied on a microscopic level, while the change in contact angle can be observed on a macroscopic level. Essentially the figure is showing that on a microscopic level the surface is rough consisting of a series of peaks and valleys. It is shown in the figure that as the flow

increases the contact line moves down from the top of a peak, along the angled surface. Thus the contact angle can be maintained locally while the apparent contact angle changes to support the increased flow. The concept locally for bubble detachment, is the contact line will move down the slope increasing the apparent contact angle. This will take place until the contact line reaches a limiting point, such that further increase in the contact line will only decrease the apparent contact angle. At this point any further increase in flow will cause the bubble to detach.

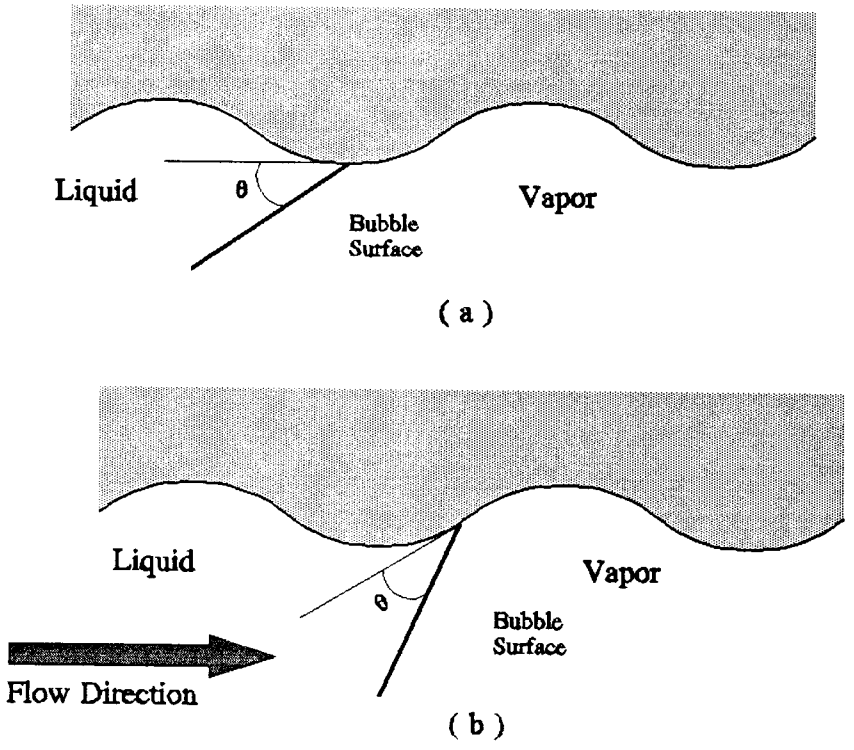

Figure 30. Contact angle hysteresis

Through the theory of contact angle hysteresis, Youngs

equation and the observation of contact angle change are in agreement. Note the forgoing is a simplified presentation on what is happening at the microscopic level. Other factors that may influence contact angle hysteresis are chemical contamination or solutes. For a detailed analysis refer to Liquid Vapor Phase Change Phenomena (Carey, 1992), Wetting Spreading and Adhesion (Padday, 1978), or De Gennes paper on wetting (De Gennes, 1985).

The observation that the apparent contact angle approaches 90 degrees before bubble detachment, even though correct for the experimentation, may not always be the correct detachment contact angle. From the forgoing analysis, the bubble may detach before the apparent upstream contact angle becomes 90 degrees. The reason for this might result from the surface being very smooth, or the microscopic contact angle being very small as a result of low surface tension. This implies another coefficient is needed in the above velocity equation. This coefficient should be a function of surface roughness and surface tension. It follows the correct detachment equation is:

$$V = C_{RS}\sqrt{\frac{4\sigma\ sin2\theta}{\pi d\ C_D\ \rho}}$$

Where:

C_{RS} = the roughness / surface tension coefficient

The above equation will be referred to as the velocity

detachment equation. Note for the experiments performed the roughness / surface tension coefficient was found to be one, for the surface roughness of 3000-6000 angstroms.

Since the velocity detachment equation results from a scale analysis of the forces on the bubble, it can be used to determine what are, and the relationship between, the critical parameters involved in bubble detachment. Five independent parameters emerge from the equation, excluding surface roughness. Those are fluid flow, bubble diameter, surface tension, fluid density, and fluid viscosity in the form of the drag coefficient. These were the five critical parameters measured in the experimentation, thus the rational for measuring these parameters is supported by scale analysis. To confirm the validity of this rough scale analysis, a comparison can be made between it and the experimental results. If the theoretical calculations match the results within an order of magnitude, and particular trends predicted are seen in the experimentation, the implication is a correct scale analysis.

COMPARISON BETWEEN THEORETICAL SCALE ANALYSIS AND EXPERIMENTAL RESULTS

From the theoretical scale analysis we have an expression, the velocity detachment equation, that predicts the fluid velocity necessary for bubble removal. To give credibility to this equation, and thus the scale analysis, predictions from this equation should be compared to the experimental results. The velocity detachment equation can be written as a relationship between any two of the critical parameters, if the other three are known or constant. In the experiments, for a each fluid, the dependant parameter was velocity while the independent parameter was the bubble diameter. Thus a good starting point for comparison would be to compare the predicted detachment velocity to the experimental velocity.

Detachment Velocity

Figures 31-36 are plots of the average channel velocity, for bubble detachment, versus the bubble diameter. The figures show both the predicted and experimental values for the velocity. In the figure titles, given fluid numbers are the same as in table 2. To calculate the predicted velocity, measured values of bubble diameter, surface tension, density, and viscosity, were used in the velocity detachment equation. Also a constant drag coefficient of .8

was assumed for the low and moderately viscous fluids (1cp, 2.8cp and 3.8cp), and a coefficient of 20 was assumed for the highly viscous fluid (19.6cp). The drag coefficients were based on that of a solid sphere for a particular Reynolds number, refer to Welty Wicks and Wilson (Welty, 1984). This basis may introduce some error, since the surface of the bubble is not solid, however it should be close enough to give reasonable results. It must be noted that in the velocity detachment equation the contact angle for the bubble is also required. Since the contact angle lens was not of sufficient resolution to obtain this contact angle, it was necessary to estimate using an equation based on the surface tension of the fluid.

The Laplace equation of capillarity for the liquid meniscus near a vertical wall gives a contact angle surface tension based equation, see Wetting Spreading and Adhesion (Padday, 1978). The Laplace equation can be integrated to yield.

$$\sin\theta = 1 - \frac{\Delta\rho\, gh^2}{2\sigma_{LV}}$$

Where:

$\Delta\rho$ = the density difference between liquid and vapor

g = gravity

h = the capillary rise

σ_{LV} = the liquid-vapor surface tension

θ = the contact angle

In the experimentation h, the capillary rise, was not measured thus it was necessary to do a rough estimation for this value, based on the contact angle in water. It was assumed for the comparison calculations that h changed little for the different fluids. Thus the contact angle could be determined as a function of surface tension. This is "rough" way to determine the contact angle for the velocity detachment equation, however, the results indicate the values obtained were close to the actual values.

It also must be noted the velocity detachment equation gives only an estimate for the local average velocity. To calculate the average channel velocity, a parabolic flow profile was assumed, and the equation used in the experimental results section for bubble velocity was solved for average channel velocity. Thus the following equation was used.

$$V_{avechannel} = .552\ V_{cal}\ \left(\frac{2d}{W} - \frac{4d^2}{3W^2}\right)^{-1}$$

Where:

W = the channel width

V_{cal} = V from the velocity detachment equation

d = the bubble diameter

Figures 31-36 show agreement between the predicted detachment velocity and the experimental velocity. In all cases the predicted value is well within an order of magnitude of the experimental. In fact the calculated

curves generated lie on, or are close to, the experimental data. Also the trends seen in the experimental values are repeated in the calculated values. Both the calculated and the experimental show an exponential increase in detachment velocity with decreasing bubble diameter. The only real deviation seen of the calculated values to the experimental, is in general the calculated predict a slightly higher value of velocity for the lower diameters and a slightly lower velocity for higher diameters. This deviation could be explained by the fact that in the calculations the drag coefficient was assumed to be constant with bubble diameter. It is possible the coefficient changes slightly with bubble diameter due to the changing velocity profile, thus resulting in the deviations seen between the calculated and the experimental results. However, in general there is agreement between the calculated and experimental results, thus giving credibility to the scale analysis used and the resulting velocity detachment equation.

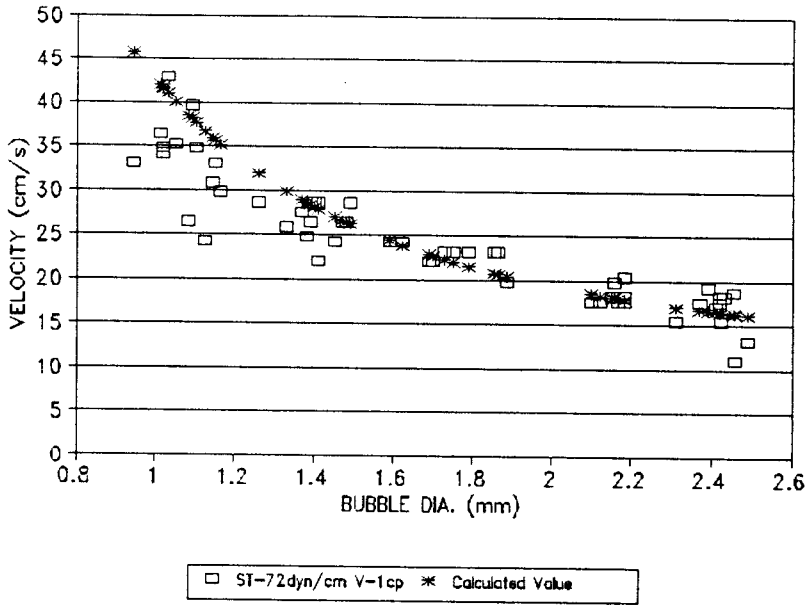

Figure 31. Channel velocity vs. bubble diameter - fluid 1 (calculated and experimental)

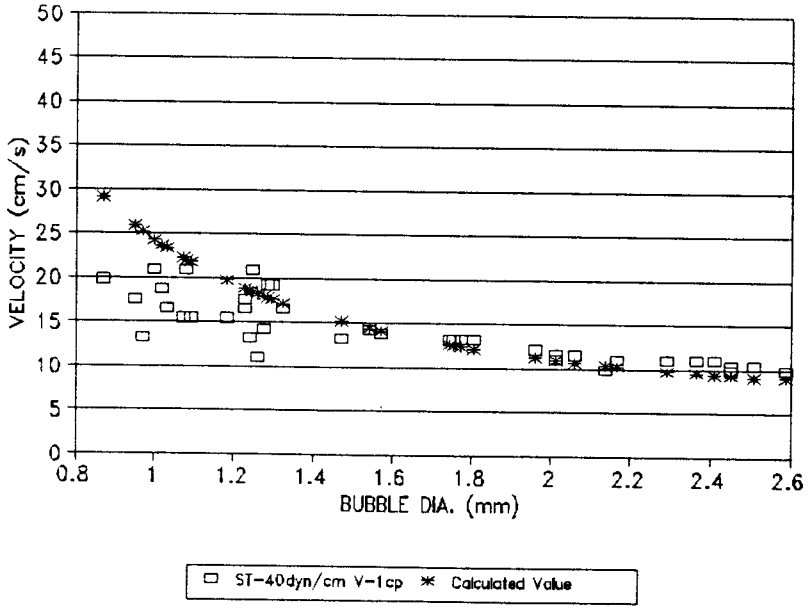

Figure 32. Channel velocity vs. bubble diameter - fluid 2 (calculated and experimental)

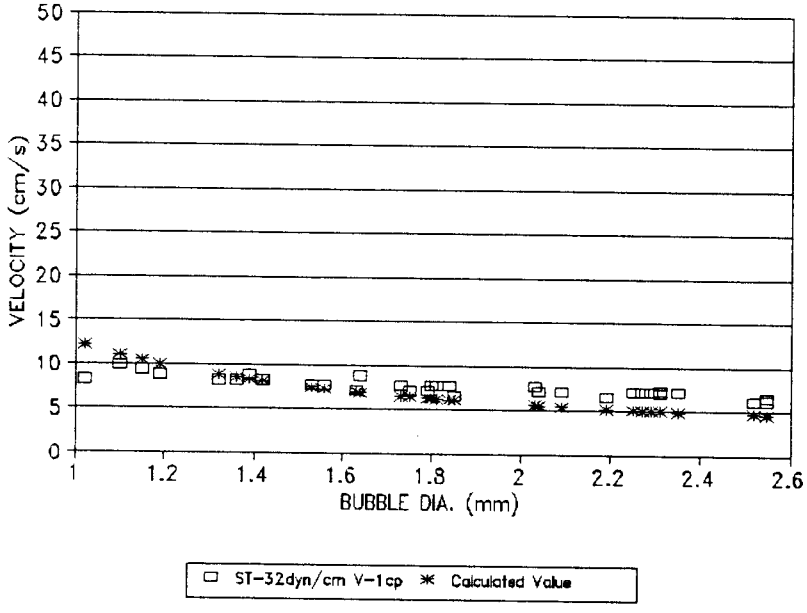

Figure 33. Channel velocity vs. bubble diameter - fluid 3 (calculated and experimental)

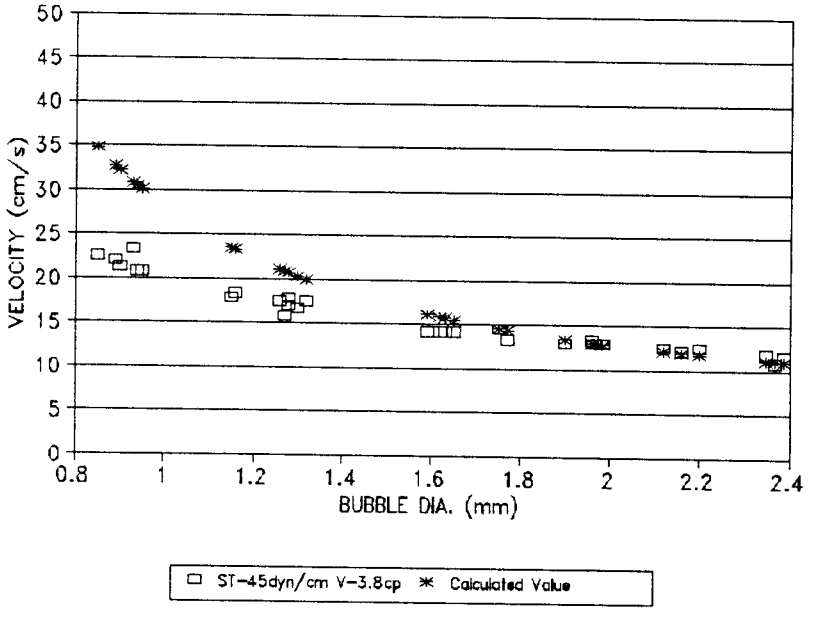

Figure 34. Channel velocity vs. bubble diameter - fluid 4 (calculated and experimental)

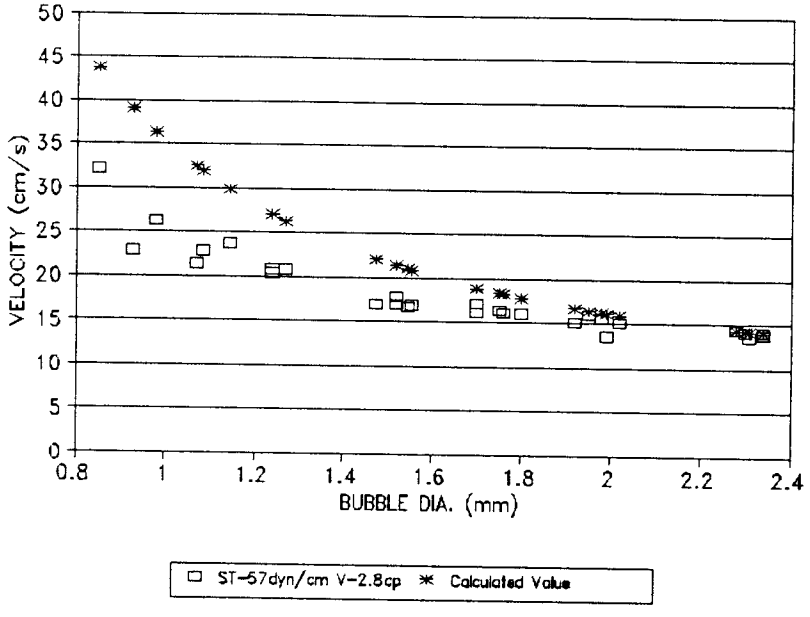

Figure 35. Channel velocity vs. bubble diameter - fluid 5 (calculated and experimental)

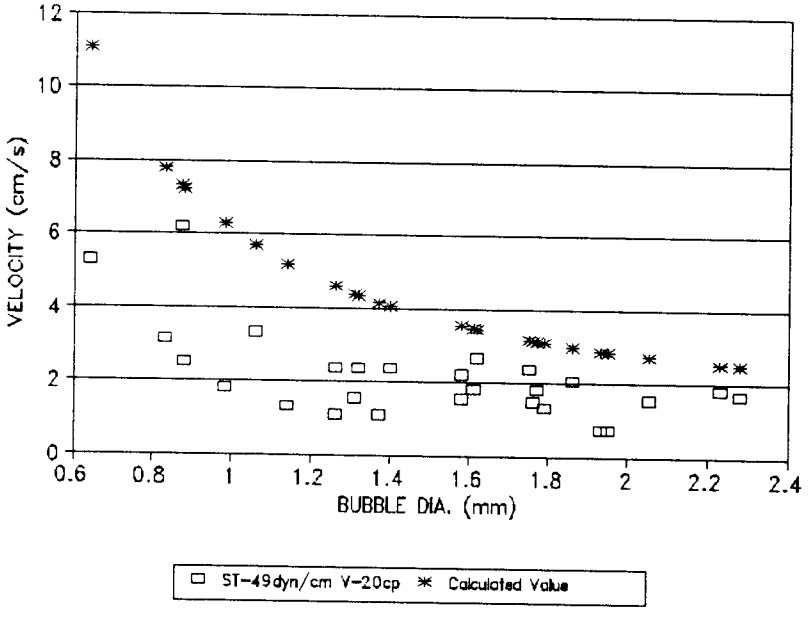

Figure 36. Channel velocity vs. bubble diameter - fluid 6 (calculated and experimental)

Weber Number versus Non-dimensional Bubble Diameter

For further comparison of the theoretical analysis to the experimental results, figures 37-41 are plots of the Weber number, based on the local velocity, versus the non-dimensional bubble diameter. These figures are of the low and moderately viscous fluids, since for the highly viscous fluid the plot of Weber number versus bubble diameter was considered to be nonviable. In the figure titles, given fluid numbers are the same as in table 2. Also, calculated values are again presented with the experimental results. The Weber number was calculated using the measured values for surface tension, bubble diameter, and density, and the calculated value of local velocity from the bubble detachment equation. The value obtained for the Weber number was a constant. This reason for this, results from using the velocity detachment equation in the Weber number equation, assuming the drag coefficient is constant. The following is the calculated Weber number equation:

$$We = \frac{4\ sin2\theta}{C_d\ \pi}$$

Note this equation states the calculated Weber number for bubble detachment is a ratio dependant on the surface tension, in the form of the contact angle, and viscosity of the fluid , in the form of the drag coefficient.

In figures 37-41 scale analysis agreement is seen between the calculated and experimental results, with the

calculated Weber number being in the middle or upper half of the range found for the experimental Weber number. The exception is figure 41 where the calculated Weber number is at the top of the experimentally found range. The general deviation seen between the calculated value and the experimental values, is that for smaller bubble diameters a higher Weber number is predicted, while for the larger bubble diameters a lower Weber number is predicted. Again, as with the velocity plots, this could be explained by noting the drag coefficient was assumed constant. If, however, the drag coefficient was slightly larger for lower bubble diameters and slightly less for larger diameters, the calculated results might be consistent with the experimental ones.

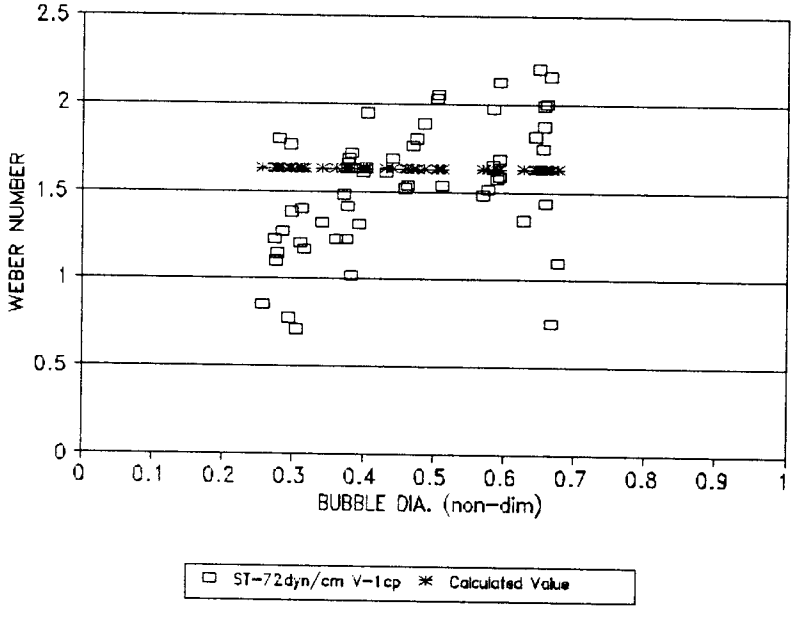

Figure 37. We vs. non-dim. bubble dia. - fluid 1 (calculated and experimental)

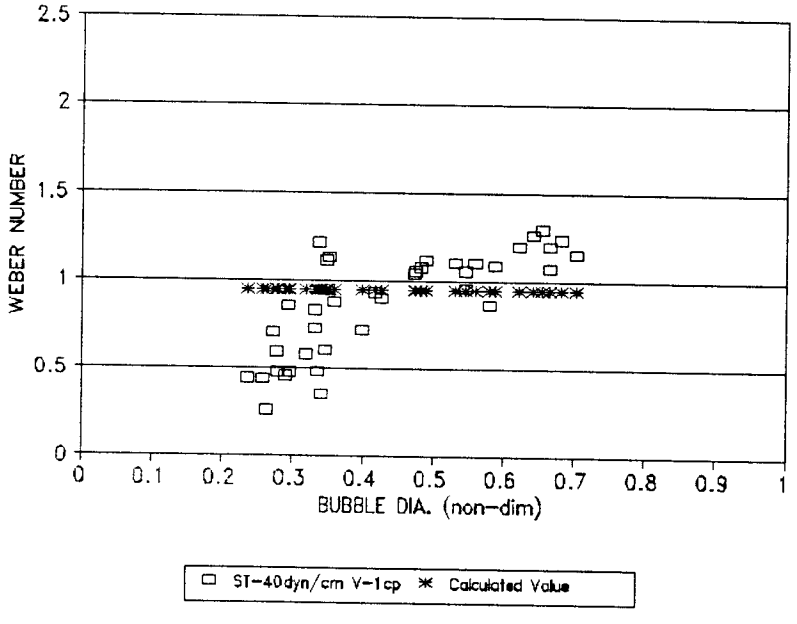

Figure 38. We vs. non-dim. bubble dia. - fluid 2 (calculated and experimental)

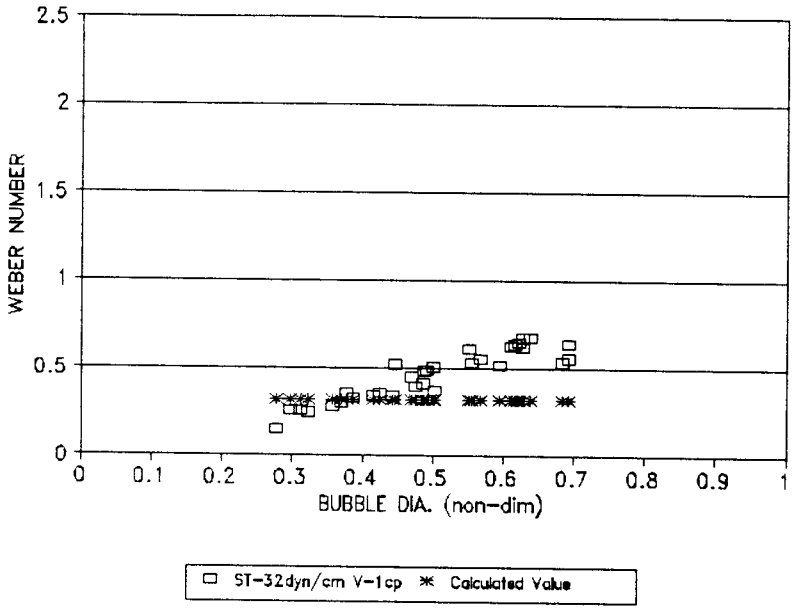

Figure 39. We vs. non-dim. bubble dia. - fluid 3 (calculated and experimental)

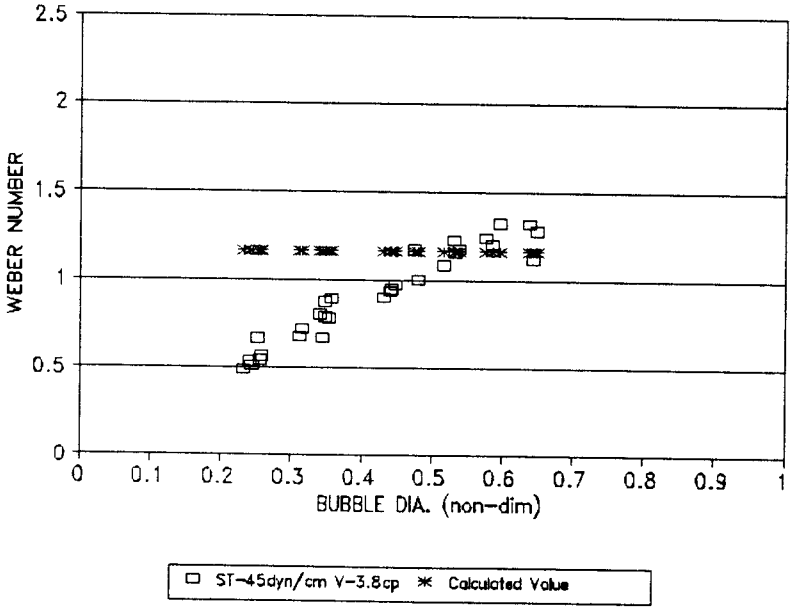

Figure 40. We vs. non-dim. bubble dia. - fluid 4 (calculated and experimental)

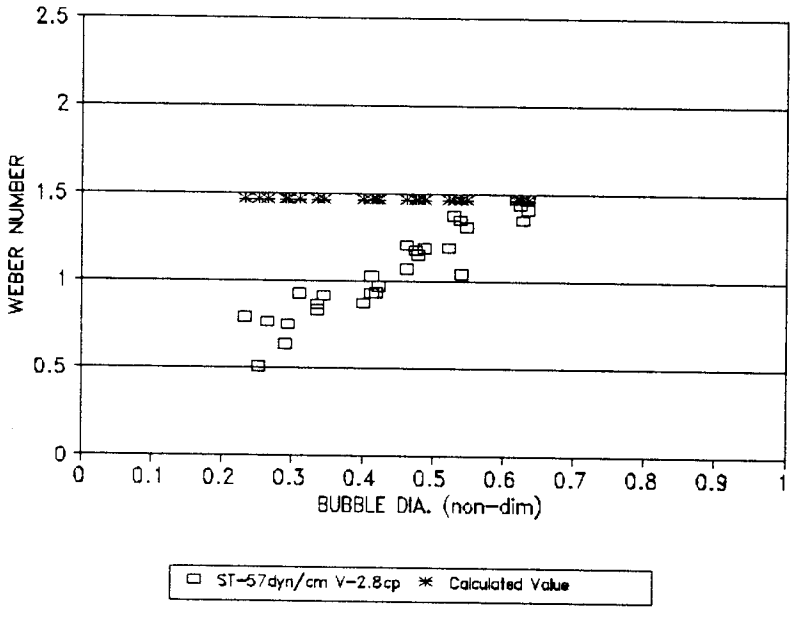

Figure 41. We vs. non-dim. bubble dia. - fluid 5 (calculated and experimental)

Weber versus Reynolds Number

To show the general trend of increasing Weber number with increasing values of the surface tension, for the low and moderately viscous fluids, figure 42 is presented. Figure 42 is a plot of the calculated Weber number versus Reynolds number, where the calculated Reynolds number is multiplied by the viscosity scale ratio. The figure shows the bulk increase in Weber number with Reynolds number. If figure 42 is compared to figure 16, it appears the average experimental value for the Weber number compares well with the calculated value, however figure 42 does not show the linear increase, for each fluid, seen from the experimentation. In fact the Weber number is constant. This difference between experimentation and calculations, is again most likely the result of assuming the drag coefficient constant. If the drag coefficient changed as function of bubble diameter this difference should disappear. In any case the general experimental trend of increasing Weber number with surface tension, is seen in the "rough" calculations of Weber number from the theoretical scale analysis section.

Comments on Comparison

The goal of this section was to give credibility to the theoretical scale analysis by comparing it to the experimental results. The comparisons presented indicate

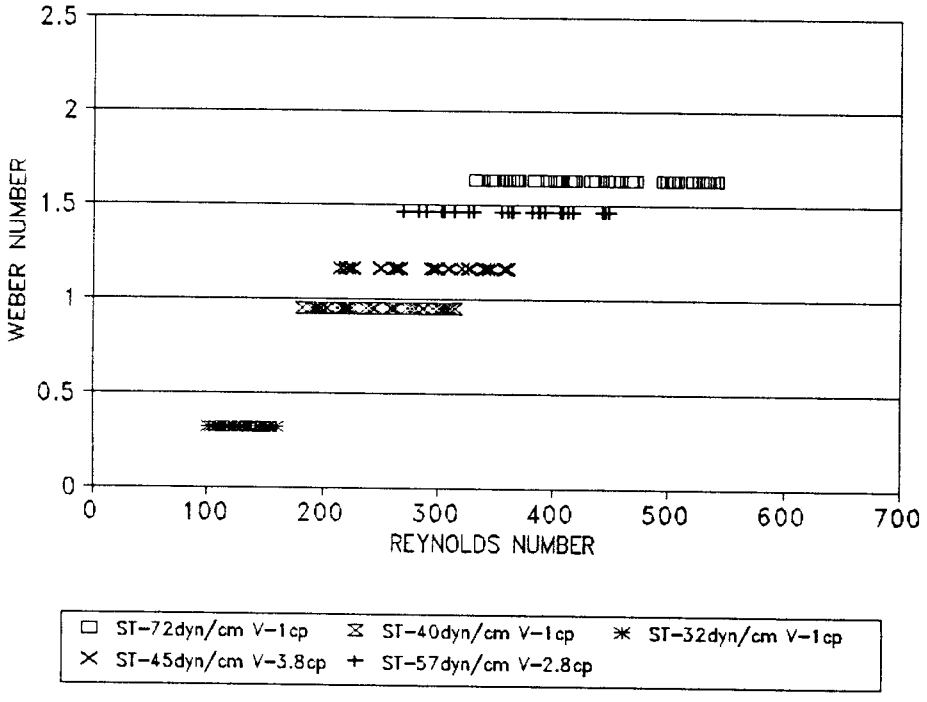

Figure 42. Calculated values for We vs. Re - fluids 1-5

that in general the performed scale analysis was correct. The results from scale analysis were able to predict values for the Weber number, and average channel detachment velocities, that were reasonably close to the experimental values. Also the analysis predicted correct trends that were seen in the different experimental plots. The main discrepancies seen between the calculated data and the experimental were most likely due to the assumption of constant drag coefficient, which was an assumption made to perform the calculations. In any case, the implication of

the scale analysis being correct means the critical parameters of surface tension, viscosity, density, bubble diameter, and fluid flow rate are the parameters involved in bubble detachment. Also it implies the velocity detachment equation gives the relationship between these parameters for bubble detachment.

COMPUTATIONAL SIMULATION

To obtain a better visualization of the flow phenomenon affecting bubble detachment a two dimensional flow simulation was performed using a computational analysis package. The package used was the FIDAP finite element analysis program (Fluid, 1991). The computational simulation consisted of steady state flow in a rectangular flow channel, with a solid half circle representing a bubble, attached to one side. The results from this simulation are presented in figures 43 and 44.

Figure 43 shows the pressure distribution on the solid half cylinder and throughout the channel. The lines in the figure represent lines of constant pressure. What is noticed when viewing the figure is the pressure is highest on the upstream face of the solid cylinder and lowest on the top of the cylinder. Also it is noticed the pressure is relatively unchanged on the downstream side of the cylinder. This agrees with experimental observations. The Young-Laplace equation indicates that an increase in pressure results in a decrease in curvature, while a decrease in pressure results in increased curvature. It is seen experimentally that when flow is increased in the chamber, curvature on the upstream side of the bubble decreases while curvature on the top increases, and the curvature on the downstream side remains the same, refer to the Experimental

section.

Figure 44 shows the flow distribution around the cylinder. The lines in the figure indicate flow stream lines. What is noticed from the figure is the flow increases over the top of the bubble and recirculates behind the bubble. This again agrees with experimental observations, since as flow in the chamber increased recirculation was noticed behind the bubble, refer to the Experimental section.

It must be noted that because the computer simulation was two dimensional, the results will not quantitatively match the actual three dimensional situation. However, the results are useful in showing the general pressure and flow phenomenon involved in bubble detachment. A three dimensional computer simulation could be used to give a more realistic quantitative depiction of the flow phenomenon. In the section on Comparison of Theoretical Calculations to Experimental Results, it was concluded the reason for the deviation of theoretical from experimental was due to the assumption of a constant drag coefficient. By performing a three dimensional simulation it may be possible to determine the drag coefficients dependance on diameter. Also in the section it was noted that the drag coefficient was for a solid sphere, while in reality the bubble surface is not solid. A three dimensional simulation, modeling the actual surface, could also give better values for the drag

coefficient. This would allow for more accurate theoretical predictions.

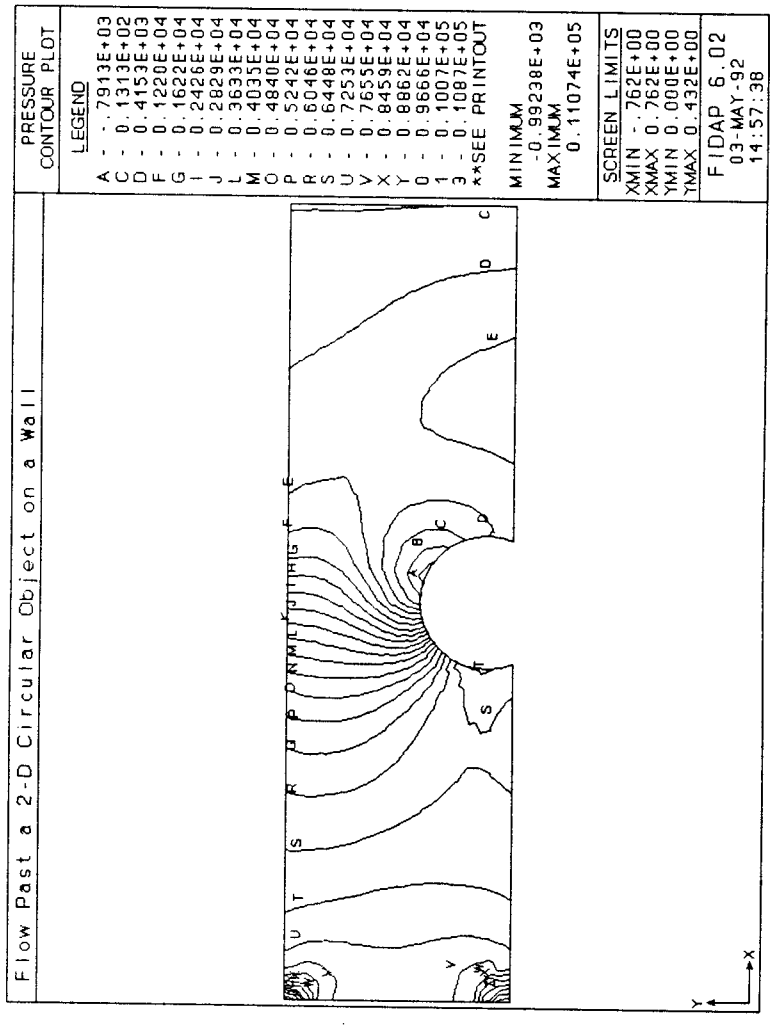

Figure 43. Pressure distribution on solid half cylinder

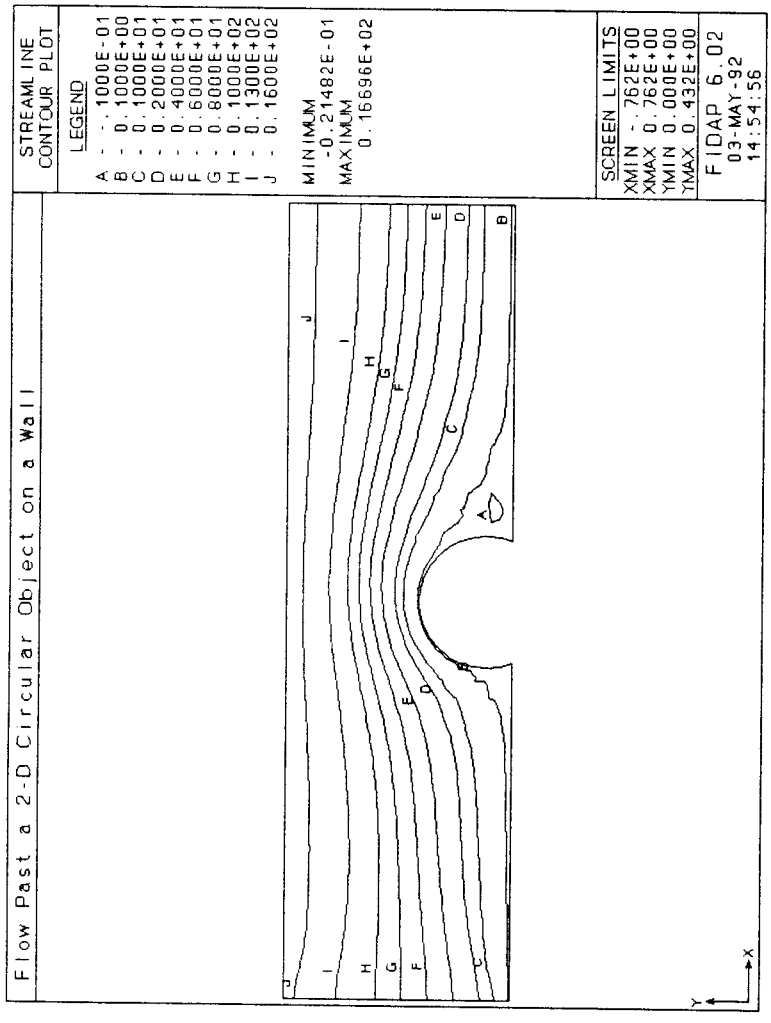

Figure 44. Flow distribution around solid half cylinder

CONCLUSION

The goal of this thesis was to determine the critical parameters involved in the dislodgement and deformation of microbubbles in laminar channel flow. The motivation behind analyzing this phenomenon, as mentioned in the introduction, comes from many areas of science and industry where interference of liquid flow by a gaseous phase, in the form of a bubble, can have a detrimental effect. A particular example is in the field of ink jet printing where a single bubble can have a disastrous effect, due to its interference in ink flow from the printer. By knowing the critical parameters involved in bubble dislodgement and deformation, and analyzing how they interrelate, predictions can be made as to when and under what conditions dislodgement and deformation occur.

To determine these critical parameters and their interrelations a four part approach was taken, of which the thesis documented. The four part approach consisted of apparatus development, experimentation, theoretical scale analysis, and a brief computational simulation. By initially performing a theoretical scale analysis, it was determined the critical parameters involved in bubble dislocation and deformation were fluid flow rate, liquid-vapor surface tension, fluid viscosity, bubble diameter, and fluid density. An apparatus and test procedure were

developed to independently vary these critical parameters and observe their effect on bubble detachment and deformation. The data from this experimentation, 219 test runs in all, were recorded and processed. The experimental data was presented, in non-dimensional parameter form, as plots of Weber versus Reynolds number, and Weber number versus non-dimensional bubble diameter. By presenting the data in this non-dimensional form the hope was for its applicability to be extended beyond the fluids experimented upon. An in-depth theoretical scale analysis was developed, based partially on experimental observations, to predict how the various parameters affect each other. The resulting analysis produced the velocity detachment equation, which indicates how the parameters are interrelated. For verification of the theoretical analysis, experimental results were compared to that generated from the velocity detachment equation. It was found the calculated data matched the experimental results, thus giving validity to the theoretical calculations. A computer simulation was performed to give insight on the flow patterns and pressure distributions effecting the bubble. This simulation gave results that were verified by experimental observations.

The goal of the thesis, to find the critical parameters involved in microbubble dislodgement and deformation and determine their relationship, was accomplished. With the development of the velocity detachment equation,

theoretically the critical parameters were determined and a relationship was given for them. Experimentally the non-dimensional plots of Weber versus Reynolds number and Weber versus the non-dimensional bubble diameter also gave the critical parameters and their relationship. By using these two results one should be able to get a rough estimate of bubble detachment.

It must be noted this was not a complete study in bubble dislocation and deformation. In the study, only one surface was used, and it was only in the horizontal position. Also most of the fluids tested were of low to moderate viscosity, only one fluid tested had high viscosity. Because of these limitations there are areas that should be further researched. Experimentally, multiple surfaces should be investigated to determine the effect of surface roughness, thus possibly determining the roughness/surface tension coefficient. The bubble attachment surface should be at angular orientations other that horizontal, so that the effect of buoyancy can be evaluated. Fluids with different high viscosities, should be tested to experimentally see the trend effect of different high viscosities. Another area for further research is that of computer simulations. By doing a three dimensional simulation of flow past a gaseous phase bubble attached to a wall, a fuller understanding of flow and pressure effects on a bubble could be obtained.

Microbubble dislocation and deformation is a area of interest to many people in different branches of science and industry. Hopefully this thesis has given insight on how and why this phenomenon occurs.

BIBLIOGRAPHY

1. Carey,V.P., Liquid Vapor Phase Change Phenomena, Bristol, Hemisphere Publishing Corp., 1992

2. De Gennes,P.G., Wetting: statics and dynamics, Reviews of Modern Physics, Vol. 57, No. 3, Part I, July, 1985, pp. 827-863.

3. Dussan,E.B., On the ability of drops or bubbles to stick to non-horizontal surfaces of solids. Part 2. Small drops or bubbles having contact angles of arbitrary size, Journal of Fluid Mechanics, Vol. 151, 1985, pp. 1-20.

4. Fluid Dynamics International,Inc.
500 Davis St, Suite 600
Evanston, Illinois 60201, (U.S.A.)
Revision 6, 1991.

5. Janczuk,B., and Bialopiotrowicz,T., Adhesion of an Air Bubble to Quartz Surface in Aqueous Solution of Aliphatic Amine Hydrochloride, Journal of Adhesion, Vol. 25, 1988, pp. 255-267.

6. Jansons,K.M., Moving contact lines on a two-dimensional rough surface, Journal of Fluid Mechanics, Vol. 154, 1985, pp. 1-28.

7. Miller,C.A. and Neogi,P., Interfacial Phenomena, New York, Marcel Dekker, Inc., 1985.

8. Padday,J.F., Wetting, Spreading and Adhesion, New York, Academic Press, 1978.

9. Ryskin,G. and Leal,L.G., Numerical solution of free-boundary problems in fluid mechanics. Part 2. Buoyancy-driven motion of a gas through a quiescent liquid, Journal of Fluid Mechanics, Vol. 148, 1984, pp. 19-35.

10. Welty,J.R., Wicks,C.E., and Wilson, R.E., Fundamentals of Momentum, Heat, and Mass Transfer, New York, John Wiley & Sons, 1984.

11. White,F.M., Viscous Fluid Flow, New York, McGraw- Hill, Inc., 1991.

APPENDIX

APPENDIX: MEASURED EXPERIMENTAL DATA

FLUID 1: Surface Tension 72 dyne/cm Viscosity 1 cp

RUN	BUBBLE DIA. (mm)	RECORDED BREAK OFF (gph)	CONTACT ANGLE (deg)	AVE. CHANNEL VELOCITY (cm/sec)
1	1.4	13	33	28.6484691
2	1.49	13	36	28.6484691
3	1.45	11	24	24.2410123
4	1.47	12	31	26.4447407
5	1.48	12	36	26.4447407
6	2.12	8	24	17.6298271
7	2.42	8.25	25	18.1807592
8	2.31	7	26	15.4260987
9	2.41	7.75	25	17.078895
10	2.49	6	22	13.2223703
11	2.46	5	17	11.018642
12	1.01	16.5	43	36.3615184
13	1.41	13	42	28.6484691
14	1.02	15.75	45	34.7087221
15	1.03	19.5	45	42.9727036
16	1.09	18	37	39.667111
17	1.15	15	40	33.0559259
18	1.1	15.75	40	34.7087221
19	1.05	16	36	35.2596542
20	1.37	12.5	36	27.5466049
21	1.39	13	36	28.6484691
22	1.39	12	38	26.4447407
23	1.7	10	37	22.0372839
24	1.69	10	36	22.0372839
25	1.75	10.5	36	23.1391481
26	1.885	9	36	19.8335555
27	1.885	9	36	19.8335555
28	1.855	10.5	42	23.1391481
29	1.865	10.5	42	23.1391481
30	2.15	8.25	37	18.1807592
31	2.18	9.25	41	20.3844876
32	2.18	8	35	17.6298271
33	2.18	8.25	33	18.1807592
34	2.42	8	32	17.6298271
35	2.37	8	31	17.6298271
36	0.945	15	30	33.0559259
37	1.083	12	31	26.4447407
38	1.016	15.5	30	34.15779
39	1.26	13	30	28.6484691
40	1.143	14	30	30.8521975
41	1.123	11	27	24.2410123
42	1.163	13.5	30	29.7503333

RUN	BUBBLE DIA. (mm)	RECORDED BREAK OFF (gph)	CONTACT ANGLE (deg)	AVE. CHANNEL VELOCITY (cm/sec)
43	1.33	11.75	30	25.8938086
44	1.38	11.25	30	24.7919444
45	1.41	10	30	22.0372839
46	1.59	11	30	24.2410123
47	1.624	11	29	24.2410123
48	1.624	11	29	24.2410123
49	1.73	10.5	29	23.1391481
50	1.73	10.5	29	23.1391481
51	1.79	10.5	29	23.1391481
52	2.098	8	29	17.6298271
53	2.166	8	29	17.6298271
54	2.156	9	29	19.8335555
55	2.43	8.25	36	18.1807592
56	2.39	8.75	31	19.2826234
57	2.424	7	31	15.4260987
58	2.454	8.5	30	18.7316913

FLUID 2: Surface Tension 40 dyne/cm Viscosity 1 cp

59	0.97	6	34	13.2223703
60	1.09	7	33	15.4260987
61	1.18	7	33	15.4260987
62	1.26	5	30	11.018642
63	1.24	6	35	13.2223703
64	1.08	9.5	34	20.9354197
65	1.245	9.5	50	20.9354197
66	1.285	8.75	38	19.2826234
67	1.295	8.75	41	19.2826234
68	0.95	8	41	17.6298271
69	1	9.5	41	20.9354197
69	0.87	9	38	19.8335555
70	1.07	7	41	15.4260987
71	1.03	7.5	41	16.5279629
72	1.02	8.5	41	18.7316913
73	1.225	8	40	17.6298271
74	1.275	6.5	37	14.3242345
75	1.225	7.5	40	16.5279629
76	1.325	7.5	36	16.5279629
77	1.47	6	42	13.2223703
78	1.57	6.25	39	13.7733024
79	1.54	6.5	39	14.3242345
80	1.745	6	39	13.2223703
81	1.755	6	39	13.2223703
82	1.805	6	38	13.2223703
83	1.775	6	39	13.2223703

RUN	BUBBLE DIA. (mm)	RECORDED BREAK OFF (gph)	CONTACT ANGLE (deg)	AVE. CHANNEL VELOCITY (cm/sec)
84	2.01	5.25	36	11.569574
85	2.01	5	37	11.018642
86	1.96	5.5	39	12.1205061
87	2.06	5.25	41	11.569574
88	2.365	5	43	11.018642
89	2.165	5	41	11.018642
90	2.135	4.5	36	9.91677776
91	2.29	5	41	11.018642
92	2.45	4.5	41	9.91677776
93	2.45	4.75	41	10.4677099
94	2.41	5	41	11.018642
95	2.59	4.5	45	9.91677776
96	2.51	4.75	46	10.4677099

FLUID 3: Surface Tension 32 dyne/cm Viscosity 1 cp

97	1.1	4.5	26	9.91677776
98	1.15	4.25	26	9.36584566
99	1.02	3.75	23	8.26398146
100	1.19	4	28	8.81491356
101	1.39	4	27	8.81491356
102	1.32	3.75	26	8.26398146
103	1.42	3.75	25	8.26398146
104	1.36	3.75	25	8.26398146
105	1.64	4	33	8.81491356
106	1.53	3.5	26	7.71304937
107	1.56	3.5	27	7.71304937
108	1.63	3.25	26	7.16211727
109	2.09	3.25	27	7.16211727
110	2.19	3	25	6.61118517
111	2.04	3.25	26	7.16211727
112	2.04	3.25	26	7.16211727
113	2.55	3	28	6.61118517
114	2.55	3	28	6.61118517
115	2.52	2.75	26	6.06025307
116	2.55	2.8	28	6.17043949
117	2.03	3.5	28	7.71304937
118	1.73	3.5	26	7.71304937
119	1.81	3.5	26	7.71304937
120	1.75	3.25	24	7.16211727
121	1.84	3.5	24	7.71304937
122	2.25	3.25	25	7.16211727
123	2.25	3.25	26	7.16211727
124	2.29	3.25	26	7.16211727
125	2.31	3.3	27	7.27230369

RUN	BUBBLE DIA. (mm)	RECORDED BREAK OFF (gph)	CONTACT ANGLE (deg)	AVE. CHANNEL VELOCITY (cm/sec)
126	1.79	3.25	28	7.16211727
127	1.85	3	25	6.61118517
128	1.8	3.5	25	7.71304937
129	1.8	3.5	26	7.71304937
130	2.25	3.25	28	7.16211727
131	2.27	3.25	30	7.16211727
132	2.31	3.15	27	6.94174443
133	2.35	3.25	30	7.16211727

FLUID 4: Surface Tension 45 dyne/cm Viscosity 3.8 cp

134	1.158	11	40	18.3480222
135	1.3	10	38	16.6800202
136	1.27	9.5	36	15.8460192
137	1.15	10.75	37	17.9310217
138	1.28	10.2	37	17.0136206
139	1.63	8.5	34	14.1780172
140	1.59	8.5	36	14.1780172
141	1.65	8.5	38	14.1780172
142	1.77	8	38	13.3440161
143	1.62	8.5	36	14.1780172
144	1.28	10.75	38	17.9310217
145	1.26	10.5	39	17.5140212
146	1.32	10.5	38	17.5140212
147	0.9	12.75	38	21.2670257
148	0.89	13.25	38	22.1010267
149	0.93	14	38	23.3520283
150	0.94	12.5	39	20.8500252
151	0.85	13.5	38	22.5180272
152	0.95	12.5	36	20.8500252
153	1.9	7.75	40	12.9270156
154	1.96	8	37	13.3440161
155	1.964	7.75	38	12.9270156
156	1.984	7.75	35	12.9270156
157	1.752	8.75	35	14.5950177
158	2.16	7.25	38	12.0930146
159	2.2	7.5	34	12.5100151
160	2.39	6.9	38	11.5092139
161	2.35	7.1	37	11.8428143
162	2.37	6.5	37	10.8420131
163	2.12	7.5	33	12.5100151

FLUID 5: Surface Tension 57 dyne/cm Viscosity 2.8 cp

RUN	BUBBLE DIA. (mm)	RECORDED BREAK OFF (gph)	CONTACT ANGLE (deg)	AVE. CHANNEL VELOCITY (cm/sec)
164	1.145	12.2	40	23.7103104
165	1.085	11.75	40	22.8357498
166	1.24	10.7	43	20.7951083
167	1.27	10.7	40	20.7951083
168	1.24	10.5	39	20.4064147
169	1.52	8.75	42	17.0053456
170	1.545	8.6	42	16.7138254
171	1.52	9.2	39	17.8799062
172	1.475	8.75	40	17.0053456
173	1.555	8.7	42	16.9081722
174	1.8	8.25	41	16.0336116
175	1.7	8.3	38	16.130785
176	1.7	8.8	36	17.102519
177	1.76	8.3	39	16.130785
178	1.75	8.45	38	16.4223052
179	2.02	7.75	37	15.0618775
180	1.95	8.2	37	15.9364382
181	1.99	7	40	13.6042765
182	1.92	7.75	43	15.0618775
183	1.98	8	41	15.5477445
184	2.34	7.1	40	13.7986233
185	2.3	7.25	37	14.0901435
186	2.31	7	42	13.6042765
187	2.34	7.25	38	14.0901435
188	2.28	7.4	38	14.3816637
189	1.07	11	38	21.3781487
190	0.98	13.5	36	26.2368189
191	0.85	16.5	32	32.0672231
192	0.928	11.75	35	22.8357498

FLUID 6: Surface Tension 49 dyne/cm Viscosity 19.6 cp

193	1.06	8	28	3.32712923
194	1.26	6.5	29	2.36391635
195	0.83	7.75	29	3.15571631
196	0.87	11.5	26	6.18376263
197	1.14	4.5	29	1.32328718
198	1.79	4.5	29	1.32328718
199	0.88	6.75	27	2.51357439
200	0.64	10.5	28	5.28056213
201	0.98	5.5	28	1.80879396
202	1.31	5	26	1.55733862
203	1.26	4	27	1.10663965
204	1.32	6.5	28	2.36391635
205	1.58	6.25	28	2.21860929

RUN	BUBBLE DIA. (mm)	RECORDED BREAK OFF (gph)	CONTACT ANGLE (deg)	AVE. CHANNEL VELOCITY (cm/sec)
206	1.37	4	28	1.10663965
207	1.77	5.5	28	1.80879396
208	1.61	5.5	27	1.80879396
209	1.75	6.5	30	2.36391635
210	1.62	7	27	2.66758341
211	1.58	5	26	1.55733862
212	1.76	4.85	26	1.48529578
213	2.23	5.5	27	1.80879396
214	2.28	5.25	27	1.6808908
215	1.95	3	28	0.72555631
216	2.05	5	27	1.55733862
217	1.86	6	27	2.0776532
218	1.93	3	27	0.72555631
219	1.4	6.5	27	2.36391635

EXPERIMENTAL DATA FOR FLOW METER CALIBRATION

FLUID 4: Surface Tension 45 dyne/cm Viscosity 3.8 cp

Flow Rate (GPH)	Actual Amount (ml)	Time (sec)
5	250	64.9
5	250	64.48
5	250	64.29
5	250	64.71
10	500	61.15
10	500	61.41
10	500	61.04
10	500	61

Equation used for actual GPH:

Act GPH= .7569 * (Rec GPH)

FLUID 5: Surface Tension 57 dyne/cm Viscosity 2.8 cp

Flow Rate (GPH)	Actual Amount (ml)	Time (sec)
5	250	54.09
5	250	53.61
5	250	53.4
5	250	53.99
10	500	54.12
10	500	53.91
10	500	53.97
10	500	54.28

Equation used for actual GPH:

Act GPH= .8819 * (Rec GPH)

FLUID 6: Surface Tension 49 dyne/cm Viscosity 19.6 cp

Flow Rate (GPH)	Actual Amount (ml)	Time (sec)
5	150	202
5	150	203
5	150	207
5	150	196
7.5	150	101
7.5	150	100
7.5	150	100
10	150	58
10	150	59
10	150	59
15	150	32
15	150	32
15	150	31.5

Equation used for actual GPH:

Act GPH = (1/1.05)*(.0166*(Rec GPH)^2 + .0656*(Rec GPH))